Astronomy & Astrophysics

Hot subdwarf stars in close-up view

I. Rotational properties of subdwarf B stars in close binary systems and nature of their unseen companions[*]

S. Geier[1], U. Heber[1], Ph. Podsiadlowski[2], H. Edelmann[1], R. Napiwotzki[3], T. Kupfer[1], and S. Müller[1]

[1] Dr. Karl Remeis-Observatory & ECAP, Astronomical Institute, Friedrich-Alexander University Erlangen-Nuremberg, Sternwartstr. 7, 96049 Bamberg, Germany
e-mail: geier@sternwarte.uni-erlangen.de
[2] Department of Astrophysics, University of Oxford, Keble Road, Oxford OX1 3RH, UK
[3] Centre of Astrophysics Research, University of Hertfordshire, College Lane, Hatfield AL10 9AB, UK

ABSTRACT

The origin of hot subdwarf B stars (sdBs) is still unclear. About half of the known sdBs are in close binary systems for which common envelope ejection is the most likely formation channel. Little is known about this dynamic phase of binary evolution. Since most of the known sdB systems are single-lined spectroscopic binaries, it is difficult to derive masses and unravel the companions' nature, which is the aim of this paper.

Due to the tidal influence of the companion in close binary systems, the rotation of the primary becomes synchronised to its orbital motion. In this case it is possible to constrain the mass of the companion, if the primary mass, its projected rotational velocity as well as its surface gravity are known. For the first time we measured the projected rotational velocities of a large sdB binary sample from high resolution spectra. We analysed a sample of 51 sdB stars in close binaries, 40 of which have known orbital parameters comprising half of all such systems known today.

Synchronisation in sdB binaries is discussed both from the theoretical and the observational point of view. The masses and the nature of the unseen companions could be constrained in 31 cases. We found orbital synchronisation most likely to be established in binaries with orbital periods shorter than 1.2 d. Only in five cases it was impossible to decide whether the sdB's companion is a white dwarf or an M dwarf. The companions to seven sdBs could be clearly identified as late M stars. One binary may have a brown dwarf companion. The unseen companions of nine sdBs are white dwarfs with typical masses. The mass of one white dwarf companion is very low. In eight cases (including the well known system KPD1930+2752) the companion mass exceeds 0.9 $M_\odot$, four of which even exceed the Chandrasekhar limit indicating that they may be neutron stars. Even stellar mass black holes are possible for the most massive companions. The distribution of the inclinations of the systems with low mass companions appears to be consistent with expectations, whereas a lack of high inclinations becomes obvious for the massive systems. We show that the formation of such systems can be explained with common envelope evolution and present an appropriate formation channel including two phases of unstable mass transfer and one supernova explosion. The sample also contains a candidate post-RGB star, which rotates fast despite its long orbital period. The post-RGB stars are expected to spin-up caused by their ongoing contraction. The age of the sdB is another important factor. If the EHB star is too young, the synchronisation process might not be finished yet. Estimating the ages of the target stars from their positions on the EHB band, we found PG 2345+318, which is known not to be synchronised, to lie near the zero-age extreme horizontal branch as are the massive candidates PG 1232−136, PG 1432+159 and PG 1101+249. These star may possibly be too young to have reached synchronisation.

The derived large fraction of putative massive sdB binary systems in low inclination orbits is inconsistent with theoretical predictions. Even if we dismiss three candidates because they may be too young and assume that the other sdB primaries are of low mass, PG 1743+477 and, in particular, HE 0532−4503 remain as candidates whose companions may have masses close to or above the Chandrasekhar limit. X-ray observations and accurate photometry are suggested to clarify their nature. As high inclination systems must also exist, an appropriate survey has already been launched to find such binaries.

Key words. binaries: spectroscopic – subdwarfs – stars: rotation

---

1. Introduction

Subluminous B stars (sdBs) show similar colours and spectral characteristics as main sequence stars of spectral type B, but are much less luminous. Compared to main sequence B stars the hydrogen Balmer lines in the spectra of sdBs are stronger while the helium lines are much weaker (if present at all) for the colour. The strong line broadening and the early confluence of the Balmer series is caused by the high surface gravities ($\log g \simeq 5.0-6.0$) of these compact stars ($R_{sdB} \simeq 0.1-0.3\,R_\odot$). Subluminous B stars are considered to be helium core burning stars with very thin hydrogen envelopes and masses of about half a solar mass (Heber 1986) located at the extreme end of the horizontal branch (EHB).

Subdwarf B stars are found in all Galactic stellar populations and are sufficiently common to account for the UV-upturn of early-type galaxies. Understanding the origin of the UV-upturn phenomenon hence has to await a proper understanding of the origin of the sdB stars themselves.

The discovery of short-period multi-periodic pulsations in some sdBs provided an excellent opportunity to probe the interiors of these stars using the tools of asteroseismology. They were theoretically predicted by Charpinet et al. (1996) at around the same time as they were observed by Kilkenny et al. (1997). They are characterised by low-amplitude, multi-periodic, short-period (80−600 s) light variations that are due to pressure (p)-mode oscillations. A second family of pulsating sdB stars was discovered by Green et al. (2003), again showing low-amplitude, multi-periodic pulsations, but periods are longer (2000−9000 s) and are identified as gravity (g) modes. An important recent achievement of sdB asteroseismology is the determination of the most fundamental parameter of a star, i.e. its mass (for a review see Fontaine et al. 2008).

The origin of EHB stars, however, is wrapped in mystery (see Heber 2009 for a review). The problem is how some kind of mass loss mechanism in the progenitor manages to remove all but a tiny fraction of the hydrogen envelope at about the same time as the helium core has attained the mass ($\sim 0.5\,M_\odot$) required for the helium flash. This requires enhanced mass loss, e.g. due to helium mixing driven by internal rotation (Sweigart 1997) or at the helium flash itself.

Mengel et al. (1976) demonstrated that the required strong mass loss can occur in a close-binary system. The progenitor of the sdB star has to fill its Roche lobe near the tip of the red-giant branch (RGB) to lose most of its hydrogen-rich envelope. The merger of binary white dwarfs was investigated by Webbink (1984) who showed that an EHB star can form when two helium core white dwarfs merge and the product is sufficiently massive to ignite helium.

Interest in the binary scenario was revived, when Maxted et al. (2001) determined a very high fraction of radial velocity variable sdB stars, indicating that about two thirds of the sdB stars in the field are in close binaries with periods of less than 30 days (see also Morales-Rueda et al. 2003;

Napiwotzki et al. 2004a). The companions, as far as their nature could be clarified, are mostly M dwarfs or white dwarfs. If the white dwarf companion is sufficiently massive, the merger of the binary system might exceed the Chandrasekhar mass and explode as a type Ia supernova. Indeed, Billères et al. (2000) and Maxted et al. (2000a) discovered KPD 1930+2752, a system that might qualify as a type Ia supernova progenitor (see also Geier et al. 2007).

These discoveries triggered new theoretical evolutionary calculations in the context of binary population-synthesis to identify the importance of various channels of close-binary evolution (Han et al. 2002, 2003), i.e. two phases of common-envelope ejection, stable Roche-lobe overflow and white dwarf merger.

1.1. Outline of the paper

The purpose of this paper is to clarify the nature of the unseen companions for 40 short-period sdB binaries, which comprises about half of the sdB stars in single-lined close binary systems with known periods and radial velocity amplitudes. We assumed tidally locked rotation and made use of the sdBs' gravities and projected rotational velocities.

The paper is structured in two parts. After a short review on close binary sdB stars (Sect. 2), part I (Sects. 3 to 8) describes the analysis of the sample. Besides constraining the mass of the companions and unravelling the nature of most companions as M dwarfs or typical white dwarfs, it reports the discovery of a population of eight unseen compact companions with masses exceeding 0.9 $M_\odot$ (in addition to KPD 1930+2752), some of which even exceed the Chandrasekhar limit. Accordingly, the latter should be neutron stars (NS) or black holes (BH). Even if they were massive white dwarfs, it would be surprising to find such a large fraction, as massive white dwarfs are rare. As no binary system containing an sdB plus a NS/BH is known today, we investigate potential formation scenarios in Sect. 8 and find it indeed possible to create such systems through two phases of common envelope evolution.

Our results rest on the assumption of tidally locked rotation. Therefore, part II of the paper (Sects. 9 and 11) deals with the synchronisation time scales of sdB stars in close binaries both from a theoretical point of view and from the perspective of empirical constraints. The general result is that systems with periods shorter than 1.2 d should be synchronised. Empirical evidence is available that systems with periods below 0.6 d are synchronised as is indeed the case for the systems with massive companions.

Although selection effects would favour the detection of highly inclined systems, no such system was found among those binaries with massive companions in our sample. This calls for a careful inspection of alternative explanations (Sect. 11). There are two aspects to be discussed. First, the sdB may not burn helium at all and, thus, is spun up due to ongoing contraction. Alternatively the actual evolutionary age of individual stars may be smaller than appreciated, i.e. the EHB star may just have formed only recently and the systems would therefore not be synchronised. In Sect. 12 we summarise and discuss the results.

2. Hot subdwarf binaries

Several studies aimed at determining the fraction of hot subdwarfs residing in close binary systems. Samples of hot subdwarfs have been checked for RV variations. The resulting fractions range from 39% to 78% (Green et al. 1997; Maxted et al. 2001; Napiwotzki et al. 2004a). Several studies were undertaken to determine the orbital parameters of subdwarf binaries
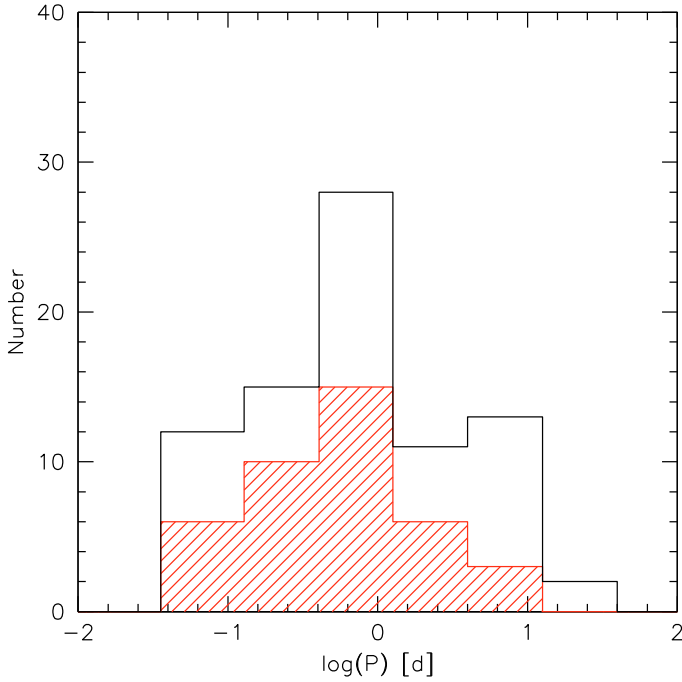
Fig. 1. Period distributions of the 40 binaries in our sample with known orbital parameters (dashed histogram) and all known 81 sdB binaries in the Ritter & Kolb (2003) catalogue (blank histogram).

(Edelmann et al. 2005; Green et al. 2008; Morales-Rueda et al. 2003, 2004; Karl et al. 2006). The orbital periods range from $0.07-30$ d with a peak at $0.5-1.0$ d (see Fig. 1).

2.1. Binary evolution

For close binary sdBs common envelope ejection is the most probable formation channel. In this scenario two main sequence stars of different masses evolve in a binary system. The heavier one will reach the red giant phase first and fill its Roche lobe. If the mass transfer to the companion is dynamically unstable, a common envelope (CE) is formed. Due to friction the two stellar cores lose orbital energy, which is deposited within the envelope and leads to a shortening of the binary period. Eventually the common envelope is ejected and a close binary system is formed, which contains a core helium-burning sdB and a main sequence companion. If this star reaches the red giant branch, another common envelope phase is possible and can lead to a close binary with a white dwarf companion and an sdB.

If the mass transfer to the companion is dynamically stable, no common envelope is formed and the primary slowly accretes matter from the secondary. The companion eventually loses most of its envelope and evolves to an sdB. This leads to sdB binaries with much larger separation and therefore much longer orbital periods. Although lots of sdBs have spectroscopically visible main sequence companions, no radial velocity variable system was detected up to now. Therefore the so called stable Roche lobe overflow (RLOF) channel remains without proof.

Binary evolution also provides a possibility to form single sdB stars via the merger of two helium white dwarfs (Webbink 1984; Iben & Tutukov 1984). Close He white dwarf binaries are formed as a result of two CE-phases. Loss of angular momentum through emission of gravitational radiation will cause the system to shrink. Given the initial separation is short enough the two white dwarfs eventually merge and if the mass of the merger is high enough, core helium burning is ignited and an sdB with very thin hydrogen envelope is formed. Recently Politano et al. (2008) proposed a new evolutionary channel. The merger of a red giant and a low mass main-sequence star during a common envelope phase may lead to the formation of a rapidly rotating hot subdwarf star. Soker (1998) proposed similar scenarios with planetary companions. A candidate substellar companion to the sdB star HD 149382 has been discovered recently (Geier et al. 2009c).

2.2. SN Ia progenitors

Double degenerate systems in close orbits are viable candidates for progenitors of type Ia supernovae (SN Ia), which play an important role as standard candles for the study of cosmic evolution (e.g. Riess et al. 1998; Leibundgut 2001; Perlmutter et al. 1999). The nature of their progenitors is still under debate (Livio 2000). The progenitor population provides crucial information for backing the assumption that distant SN Ia can be used as standard candles like the ones in the local universe.

There is general consensus that only the thermonuclear explosion of a white dwarf (WD) is compatible with the observed features of SN Ia. For this a white dwarf has to accrete mass from a close companion to reach the Chandrasekhar limit of 1.4 $M_\odot$ (Hamada & Salpeter 1961). According to the so-called double degenerate scenario (Iben & Tutukov 1984), the mass-donating companion is a white dwarf, which eventually merges with the primary due to orbital shrinkage caused by gravitational wave radiation. A progenitor candidate for the double degenerate scenario must have a total mass near or above the Chandrasekhar limit and has to merge in less than a Hubble time. Systematic radial velocity (RV) searches for double degenerates have been undertaken (e.g. Napiwotzki 2003 and references therein). The largest of these projects was the ESO SN Ia Progenitor Survey (SPY, Napiwotzki et al. 2001b). The best known double degenerate SN Ia progenitor candidate system KPD 1930+2752 has an sdB primary[1], which will become a white dwarf within about 10^8 yr before the merger occurs in about 2×10^8 yr (Maxted et al. 2000a; Geier et al. 2007). Another sdB+WD binary with massive companion has been found recently (Geier et al. 2010a).

Most recently Mereghetti et al. (2009) showed that in the X-ray binary HD 49798 a very massive ($>1.2\ M_\odot$) white dwarf accretes matter from the wind of its closely orbiting subdwarf O companion. Iben & Tutukov (1994) predicted that such a system will evolve into a SN Ia when the primary fills its Roche lobe and transfers mass to the white dwarf to reach the Chandrasekhar limit. This makes HD 49798 a candidate for SN Ia progenitor for this so called single degenerate scenario.

2.3. Nature of the companions

An up-to-date compilation of hot subdwarf binaries with known orbital parameters is presented by Ritter & Kolb (2003) which lists 81 such systems. In general it is difficult to put constraints on the nature of the close companions of sdB stars. Since most of these binaries are single-lined, only lower limits to the companion masses could be derived from the stellar mass functions, which are in general compatible with late main sequence stars

---

[1] The more massive component of a binary is usually defined as the primary. But in most close sdB binaries with unseen companions the masses are unknown and it is not possible to decide a priori which component is the most massive one. For this reason we call the visible sdB component of the binaries the primary throughout this paper.

of spectral type M or compact objects like white dwarfs. For single-lined binaries with longer orbital periods the stellar mass function can help to further constrain the nature of the unseen companion. Assuming the canonical mass (0.47 $M_\odot$; Han et al. 2002, 2003) for the subdwarf, the minimum mass of the companion may be high enough to exclude main sequence stars, because they would contribute significantly to the flux and therefore appear in the spectra. This mass limit lies near 0.45 $M_\odot$ (Lisker et al. 2005).

Twelve sdB binaries have been reported to show eclipses. A combined analysis of the light curves and time resolved spectra of these stars allows to derive the system parameters as well as the companion types. Eight of them have late M companions (see For et al. 2010 for a review), while four show shallow variations caused by the eclipse of a white dwarf (Orosz & Wade 1999; Green et al. 2004; Bloemen et al. 2010).

If close binary stars are double-lined, the mass ratio of the systems can be derived from the RV semi-amplitudes of the two components. Until recently, only one double-lined He-sdB+He-sdB binary could be analysed (Ahmad & Jeffery 2004).

Light variations can help to unravel the nature of the companion by means of the reflection effect and by ellipsoidal variations, even if there are no eclipses. In short period sdB binaries with orbital periods up to about half a day and high inclination the hemisphere of a cool main sequence or substellar companion directed towards the subdwarf is significantly heated up by the hot primary. This leads to a characteristic modulation of the light curve with the orbital period, which is a clear indication for an M-star or substellar companion. Such light variations are easily measured in short period binaries with high orbital inclinations. Fourteen sdB+M binaries with this so-called reflection effect are known so far. Since detailed physical models of the reflection effect are not available yet, several free parameters have to be adjusted to fit the observed light curves. Only very limited constraints can therefore be put on the companion masses and radii from an observed reflection effect alone. The absence of a reflection effect can also help to constrain the nature of the unseen companions (Maxted et al. 2004; Shimanskii et al. 2008). This method works best for binaries with periods of less than 0.5 d because otherwise the expected reflection effect from an M dwarf companion is hard to detect (Drechsel, priv. comm.; Napiwotzki et al., in prep.). The binary JL 82 shows a very strong reflection, because it is clearly detectable despite the long orbital period of 0.74 d. What causes the strong variation is not yet understood (Koen 2009, see also Sect. 7.1).

A massive white dwarf companion was identified as companion of an sdB (Billères et al. 2000; Maxted et al. 2000a; Geier et al. 2007), which shows a variation in its light curve caused by the tidal distortion of the sdB. Similar signs of ellipsoidal deformation could be detected in five other cases (Orosz & Wade 1999; O'Toole et al. 2006; Geier et al. 2008a; Koen et al. 2010; Bloemen et al. 2010). These stars must have white dwarf companions, because the effect of tidal distortion in the light curve is much weaker than a reflection effect, if present.

From 81 close binary subdwarfs with known orbital parameters (Ritter & Kolb 2003), 13 have bona fide M dwarf companions, while 7 companions have to be white dwarfs. In another 11 binaries compact companions are most likely. One of the binaries has a subdwarf companion. The nature of the unseen companions in the remaining 50 binaries could not be clarified with the methods described so far.

Some hot subluminous stars may not be connected to EHB-evolution at all, as exemplified by HD 188112 (Heber et al. 2003), which was found to be of too low mass to sustain helium

burning in the core. Its atmospheric parameters place the star below the EHB. An object like HD 188112 is considered to be a direct progenitor of low-mass white dwarfs (Liebert et al. 2004), which descend from the red giant branch and cool down.

2.4. Rotational properties

While the rotational properties of blue horizontal branch (BHB) stars both in globular clusters and in the field are thoroughly examined (see e.g. Behr 2003), there is no systematic study for EHB stars yet. Most of the sdB stars where $v_{\rm rot} \sin i$-measurements are available, are slow rotators (Heber et al. 2000; Napiwotzki et al. 2001a; Edelmann 2005).

The knowledge of the projected rotational velocity, combined with the gravity determination, allows to derive the mass of single-lined binaries, if the rotation is tidally locked to the orbit. A similar technique has been applied to low-mass X-ray binaries. Kudritzki & Simon (1978) made use of this method for the first time in the field of hot subdwarfs to constrain the parameters of the sdO binary HD 49798. Recently, also a few sdB systems have been studied in this way (e.g. Napiwotzki et al. 2001a; O'Toole et al. 2004; Geier et al. 2007, 2008a, 2010a). Here we apply this technique to a much larger sample.

Part I: Quantitative spectral analysis and binary evolution

Here we present our measurements of projected rotational velocities for a sample of 51 radial velocity variable sdBs stars in total. 40 of them are drawn from the Ritter & Kolb (2003) catalogue (including GD 687, a system published more recently, Geier et al. 2010a) and have well determined orbital parameters. Eleven additional radial velocity variable sdB stars have also been analysed, but orbital parameters have not yet been determined. The main aim is to constrain the masses of the companions under the assumption of tidally locked rotation.

Observations and analysis method are described in Sects. 3 and 4. Surface gravity (Sect. 5) and projected rotational velocities (Sect. 6) will be combined with the mass function to derive companion masses and inclinations. The nature of the companions is discussed Sect. 7. An evolutionary scenario for the formation of neutron star or black hole companions to sdB stars is proposed in Sect. 8.

3. Observations and data reduction

The first set of UVES spectra were obtained in the course of the ESO Supernovae Ia Progenitor Survey (SPY, Napiwotzki et al. 2001b, 2003) at spectral resolution $R \simeq 20\,000-40\,000$ covering 3200−6650 Å with two small gaps at 4580 Å and 5640 Å. Each of the 19 stars were observed at least twice. The data reduction is described in Lisker et al. (2005). For some of the systems follow-up observations with UVES in the same setup were undertaken to derive the orbital parameters. These were taken through a narrow slit for better accuracy. For the high priority target PG 1232−136 we obtained 60 short exposures (2 min) with UVES through a very narrow slit (0.4″) to achieve higher resolution ($R = 80\,000$) covering 3770−4980 Å and 5690−7500 Å.

High resolution spectra ($R = 30\,000$, 4260−6290 Å) of 12 known close binary subdwarfs have been taken with the HRS fiber spectrograph at the Hobby Eberly Telescope (HET) in the

second and third trimester 2007. The spectra were reduced using standard ESO MIDAS routines.

Another sample of 11 known bright subdwarf binaries was observed with the FEROS spectrograph ($R = 48\,000$, 3750−9200 Å) mounted at the ESO/MPG 2.2 m telescope. The spectra were downloaded from the ESO science archive and reduced with the FEROS-DRS pipeline under the ESO MIDAS context in optimum extraction mode.

Three spectra of subdwarf binaries were obtained with the FOCES spectrograph ($R = 30\,000$, 3800−7000 Å) mounted at the CAHA 2.2 m telescope. Three spectra were taken with the HIRES instrument ($R = 45\,000$, 3600−5120 Å) at the Keck telescope. Two spectra taken with the echelle spectrograph ($R = 20\,000$, 3900−8060 Å) at the 1.5 m Palomar telescope were provided by Reid (priv. comm.).

Because a wide slit was used in the SPY survey and the seeing disc did not always fill the slit, the instrumental profile of some of the UVES spectra was seeing dependent. This has to be accounted for to estimate the instrumental resolution. The seeing of all single exposures was measured with the DIMM seeing monitor at Paranal Observatory and taken from the ESO science archive (Sarazin & Roddier 1990). As a test the seeing was also estimated from the width of the echelle orders perpendicular to the direction of dispersion in some cases and found to be consistent with the DIMM measurements. The errors are considered to be lower than the change of seeing during the exposures (up to 0.′′2). The resolution of the spectra taken with the fiber spectrographs FEROS, FOCES and HRS was assumed as constant. Changes in the instrumental resolution because of temperature variations and for other reasons were considered as negligible.

The single spectra of all programme stars were RV-corrected and co-added in order to achieve higher signal-to-noise.

4. Analysis method

Since the the programme stars are single-lined spectroscopic binaries, no information about the orbital motion of the sdBs' companions is available, and thus only their mass functions can be calculated.

$$f_{\rm m} = \frac{M_{\rm comp}^3 \sin^3 i}{(M_{\rm comp} + M_{\rm sdB})^2} = \frac{PK^3}{2\pi G} \,. \tag{1}$$

Although the RV semi-amplitude K and the period P are determined by the RV curve, the sdB mass $M_{\rm sdB}$, the companion mass $M_{\rm comp}$ and the inclination angle i remain free parameters.

In the following analysis we adopt the mass range for sdBs in binaries which underwent the common envelope channel given by Han et al. (2002, 2003) if no independent mass determinations are available (see Sect. 7 for details).

In close binary systems, the rotation of the stars becomes synchronised to their orbital motion by tidal forces (see Sect. 9 for a detailed discussion). In this case their rotational periods equal the orbital periods of the binaries. If the sdB primary is synchronised in this way its rotational velocity $v_{\rm rot}$ can be calculated.

$$v_{\rm rot} = \frac{2\pi R_{\rm sdB}}{P} \,. \tag{2}$$

The stellar radius R is given by the mass-radius relation and can be derived, if the surface gravity g has been determined.

$$R = \sqrt{\frac{M_{\rm sdB} G}{g}} \,. \tag{3}$$

The measurement of the projected rotational velocities $v_{\rm obs} = v_{\rm rot} \sin i$ and the surface gravities g therefore allows to constrain the systems' inclination angles i. With $M_{\rm sdB}$ as free parameter the mass function can be solved and the inclination angle as well as the companion mass can be derived. Because of $\sin i \leq 1$ a lower limit for the sdB mass is given by

$$M_{\rm sdB} \geq \frac{v_{\rm obs}^2 P^2 g}{4\pi^2 G} \,. \tag{4}$$

This method has already been applied to the sdB+WD binaries HE 1047−0436 (Napiwotzki et al. 2001a), Feige 48 (O'Toole et al. 2004), KPD 1930+2752 (Geier et al. 2007), PG 0101+039 (Geier et al. 2008a) and GD 687 (Geier et al. 2010a).

There are no signatures of companions visible in the optical spectra of our programme stars. Main sequence stars with masses higher than 0.45 $M_\odot$ could therefore be excluded because otherwise spectral features of the cool secondary (e.g. Mg I lines at ≃5170 Å) would appear in the spectra (Lisker et al. 2005) and a flux excess in the infrared would become visible in the spectral energy distribution (Stark & Wade 2003; Reed & Stiening 2004).

Another possibility to detect M dwarf or brown dwarf companions are reflection effects in the binary light curves. The detection of a reflection effect provides solid evidence for the presence of an M dwarf or brown dwarf companion. The non-detection of such a modulation can be used to constrain the nature of the companion as well, since a compact object like a white dwarf would be too small to contribute significantly to the total flux and cause a detectable reflection effect. But constraining the companion type in this way is problematic for several reasons. First of all, the amplitude of the reflection becomes very small (a few mmag) unless the binary has a short period (<0.5 d, Drechsel, priv. comm.; Napiwotzki et al., in prep.). Unless the photometry is excellent, such shallow variations over long timescales are not detectable from the ground. Furthermore, the amplitude of the modulation depends on the binary inclination, which is not known in general. An sdB+M binary seen at very low inclination does not show a detectable reflection effect. But most importantly the physics behind the reflection effect itself is poorly understood and one has to use rather crude approximations to derive its amplitude. The most recent detection of a surprisingly strong reflection effect in the long period system JL 82 (Koen 2009) illustrates this.

Some of our programme stars have already been checked for modulations in their light curves. We consider the lack of a reflection effect as significant constraint, if the orbital period of the binary is shorter than 0.5 d. In this case the companion should be a compact object. In the case of binaries with longer periods the non-detection of a reflection effect is used as consistency check.

The atmospheric parameters effective temperature and surface gravity of most of our programme stars have been derived from low resolution spectra with sufficient accuracy and can be taken from literature in most cases. In order to measure projected rotational velocities of sdB stars however, high spectral resolution is necessary, because the $v_{\rm rot} \sin i$ are small in most cases.

5. Determination of the surface gravity and systematic errors

Since the precise determination of the atmospheric parameters, especially the surface gravity, is of utmost importance for our analysis, this section is devoted to the systematic uncertainties dominating the determination of these parameters. Spectra of

Table 1. Atmospheric and orbital parameters.

System	$T_{\rm eff}$ [K]	$\log g$	P [d]	K [km s^{-1}]	γ [km s^{-1}]	References
PG 1017−086	30 300 ± 500	5.61 ± 0.10	0.0729938 ± 0.0000003	51.0 ± 1.7	−9.1 ± 1.3	14
KPD 1930+2752	35 200 ± 500	5.61 ± 0.06	0.0950933 ± 0.0000015	341.0 ± 1.0	5.0 ± 1.0	7
HS 0705+6700	28 800 ± 900	5.40 ± 0.10	0.09564665 ± 0.00000039	85.8 ± 3.7	−36.4 ± 2.9	2
PG 1336−018	32 800 ± 500	5.76 ± 0.05	0.101015999 ± 0.00000001	78.7 ± 0.6	−25	1,23
HW Vir	28 500 ± 500	5.63 ± 0.05	0.115 ± 0.0008	84.6 ± 1.1	−13.0 ± 0.8	24,3
PG 1043+760	27 600 ± 800	5.39 ± 0.10	0.1201506 ± 0.00000003	63.6 ± 1.4	24.8 ± 1.4	13,15
BPS CS 22169−0001†	39 300 ± 500	5.60 ± 0.05	0.1780 ± 0.00003	14.9 ± 0.4	2.8 ± 0.3	25,5
PG 1432+159	26 900 ± 1000	5.75 ± 0.15	0.22489 ± 0.00032	120.0 ± 1.4	−16.0 ± 1.1	21,16
PG 2345+318	27 500 ± 1000	5.70 ± 0.15	0.2409458 ± 0.000008	141.2 ± 1.1	−10.6 ± 1.4	22,16
PG 1329+159	29 100 ± 900	5.62 ± 0.10	0.249699 ± 0.0000002	40.2 ± 1.1	−22.0 ± 1.2	13,15
HE 0532−4503	25 400 ± 500	5.32 ± 0.05	0.2656 ± 0.0001	101.5 ± 0.2	8.5 ± 0.1	10,19
CPD −64 481	27 500 ± 500	5.60 ± 0.05	0.2772 ± 0.0005	23.8 ± 0.4	94.1 ± 0.3	19,5
PG 1101+249	29 700 ± 500	5.90 ± 0.07	0.35386 ± 0.00006	134.6 ± 1.3	−0.8 ± 0.9	4,16
PG 1232−136	26 900 ± 500	5.71 ± 0.05	0.3630 ± 0.0003	129.6 ± 0.04	4.1 ± 0.3	25,5
Feige 48	29 500 ± 500	5.54 ± 0.05	0.376 ± 0.003	28.0 ± 0.2	−47.9 ± 0.1	19,20
GD 687	24 300 ± 500	5.32 ± 0.07	0.37765 ± 0.00002	118.3 ± 3.4	32.3 ± 3.0	11,9
KPD 1946+4340	34 200 ± 500	5.43 ± 0.10	0.403739 ± 0.0000008	167.0 ± 2.4	−5.5 ± 1.0	25,15
HE 0929−0424	29 500 ± 500	5.71 ± 0.05	0.4400 ± 0.0002	114.3 ± 1.4	41.4 ± 1.0	10,18
HE 0230−4323	31 100 ± 500	5.60 ± 0.07	0.45152 ± 0.00002	62.4 ± 1.6	16.6 ± 1.0	11,5
PG 1743+477	27 600 ± 800	5.57 ± 0.10	0.515561 ± 0.0000001	121.4 ± 1.0	−65.8 ± 0.8	15
PG 0001+275	25 400 ± 500	5.30 ± 0.10	0.529842 ± 0.0000005	92.8 ± 0.7	−44.7 ± 0.5	25,5
PG 0101+039	27 500 ± 500	5.53 ± 0.07	0.569899 ± 0.000001	104.7 ± 0.4	7.3 ± 0.2	8
PG 1248+164	26 600 ± 800	5.68 ± 0.05	0.73232 ± 0.000002	61.8 ± 1.1	16.2 ± 1.3	13,15
JL 82	26 500 ± 500	5.22 ± 0.10	0.73710 ± 0.00005	34.6 ± 1.0	−1.6 ± 0.8	25,5
TON S 183	27 600 ± 500	5.43 ± 0.05	0.8277 ± 0.0002	84.8 ± 1.0	50.5 ± 0.8	25,5
PG 1627+017	23 500 ± 500	5.40 ± 0.10	0.8292056 ± 0.0000014	70.10 ± 0.13	−54.16 ± 0.27	25,6
PG 1116+301	32 500 ± 1000	5.85 ± 0.10	0.85621 ± 0.000003	88.5 ± 2.1	−0.2 ± 1.1	13,15
HE 2135−3749	30 000 ± 500	5.84 ± 0.05	0.9240 ± 0.0003	90.5 ± 0.6	45.0 ± 0.5	10,18
HE 1421−1206	29 600 ± 500	5.55 ± 0.07	1.188 ± 0.001	55.5 ± 2.0	−86.2 ± 1.1	11,18
HE 1047−0436	30 200 ± 500	5.66 ± 0.05	1.21325 ± 0.00001	94.0 ± 3.0	25 ± 3.0	17
PG 0133+114	29 600 ± 900	5.66 ± 0.10	1.23787 ± 0.000003	82.0 ± 0.3	−0.3 ± 0.2	15,5
PG 1512+244	29 900 ± 900	5.74 ± 0.10	1.26978 ± 0.000002	92.7 ± 1.5	−2.9 ± 1.0	13,15
[CW83] 1735+22	38 000 ± 500	5.54 ± 0.05	1.278 ± 0.001	103.0 ± 1.5	20.6 ± 0.4	25,5
HE 2150−0238	30 200 ± 500	5.83 ± 0.05	1.321 ± 0.005	96.3 ± 1.4	−32.5 ± 0.9	11,18
HD 171858	27 200 ± 800	5.30 ± 0.10	1.63280 ± 0.000005	87.8 ± 0.2	62.5 ± 0.1	25,5
PG 1716+426	27 400 ± 800	5.47 ± 0.10	1.77732 ± 0.000005	70.8 ± 1.0	−3.9 ± 0.8	13,15
PB 7352	25 000 ± 500	5.35 ± 0.10	3.62166 ± 0.000005	60.8 ± 0.3	−2.1 ± 0.3	25,5
CD −24 731	35 400 ± 500	5.90 ± 0.05	5.85 ± 0.003	63 ± 3	20 ± 5	19,5
HE 1448−0510	34 700 ± 500	5.59 ± 0.05	7.159 ± 0.005	53.7 ± 1.1	−45.5 ± 0.8	10,18
PHL 861	30 000 ± 500	5.50 ± 0.05	7.44 ± 0.015	47.9 ± 0.4	−26.5 ± 0.4	10,18

Notes. In the last column references for the atmospheric parameters effective temperature $T_{\rm eff}$ and surface gravity $\log g$ (first number) and the orbital parameters period P, radial velocity semi-amplitude K and system velocity γ (second number) are given separately. If both parameter sets are taken from one source, only one reference number is given.

References. 1 Charpinet et al. (2008), 2 Drechsel et al. (2001), 3 Edelmann (2008), 4 Edelmann et al. (1999), 5 Edelmann et al. (2005), 6 For et al. (2006), 7 Geier et al. (2007), 8 Geier et al. (2008a), 9 Geier et al. (2010a), 10 Karl et al. (2006), 11 Lisker et al. (2005), 12 Maxted et al. (2000b), 13 Maxted et al. (2001), 14 Maxted et al. (2002), 15 Morales-Rueda et al. (2003), 16 Moran et al. (1999), 17 Napiwotzki et al. (2001a), 18 Napiwotzki et al. (in prep.) preliminary results are given in Karl et al. (2006), 19 O'Toole & Heber (2006), 20 O'Toole et al. (2004), 21 Saffer et al. (1994), 22 Saffer et al. (1998), 23 Vučković et al. (2007), 24 Wood & Saffer (1999) and this work 25 † The significance of the orbital solution given by Edelmann et al. (2005) is rather low, but the possible aliases all lie around 0.2 d.

sdB stars in the literature were analysed either with metal line-blanketed LTE model atmospheres or with NLTE model atmospheres neglecting metal line blanketing altogether. As pointed out by Heber et al. (2000), Heber & Edelmann (2004) and Geier et al. (2007), systematic differences between these two approaches are present. Most importantly the gravity scale differs by about 0.05 dex.

Most of the atmospheric parameters of our programme stars are taken from literature and were derived by fitting LTE or NLTE models (Table 1). The adopted errors in $\log g$ range from 0.05 to 0.15. It is important to note that all stars except

PG 1336−018, HW Vir, PG 1432+159 and PG 2345+318 have been analysed with the same grids of LTE and NLTE atmospheres and the same fitting procedure. The error in surface gravity starts to dominate the error budget of the derived parameters as soon as the error in $v_{\rm rot} \sin i$ drops below about 1.0 km s^{-1} (see Sect. 6).

In cases where no reliable atmospheric parameters could be found in literature, we determined them by fitting LTE models. Since the accuracy of the parameters is very much dependent on the higher Balmer lines, a high S/N in this region is necessary. The quality of high resolution spectra obtained

with FEROS or FOCES declines toward the blue end. This can cause systematic shifts in the parameter determination (up to $\Delta T_{\rm eff} \simeq 2000$ K and $\Delta \log g = 0.2$). That is why we chose UVES, HIRES or low resolution spectra to determine the atmospheric parameters if possible. In order to improve the atmospheric parameter determination of TON S 183, BPS CS 22169−0001 and [CW83] 1735+22 we obtained additional medium resolution spectra with WHT/ISIS in August 2009. A medium resolution spectrum of KPD 1946+4340 taken with ISIS (Morales-Rueda et al. 2003) and a low resolution spectrum taken with the B&C spectrograph mounted at the 2.3 m Bok telescope on Kitt Peak (Green, priv. comm.) have been fitted with metal-enriched models.

For the hot stars BPS CS 22169−0001, [CW83] 1735+22 and KPD 1946+4340 the NLTE models usually applied gave a strong mismatch for the He II line at 4686 Å. Using metal line blanketed LTE models of solar composition did not improve the fit. A similar problem was found by O'Toole & Heber (2006) in their analysis of our programme star CD −24 731 (and two other hot sdBs), which is of similarly high temperature. The problem was remedied by using metal enhanced models. Later, the same indication was found for KPD 1930+2752 (Geier et al. 2007) and AA Dor (Müller et al. 2010). For this reason we used model atmospheres of ten times solar metallicity. Although the atmospheric parameters did not change much, the He II line at 4686 Å was matched well in concert with the He I and hydrogen Balmer lines.

Only in the case of JL 82 we had to rely on FEROS spectra. Since the parameters derived from these spectra ($T_{\rm eff}$ = 25 000 K, $\log g$ = 5.20) turned out to be very similar to the ones derived from the FEROS spectra of TON S 183 ($T_{\rm eff}$ = 26 000 K, $\log g$ = 5.00), the systematic shifts ($\Delta T_{\rm eff}$ = +1500 K, $\Delta \log g$ = +0.2) should be similar as well. The parameters of JL 82 have therefore been corrected for these shifts.

Results are summarised in Table 1 and plotted in Fig. 2, where they are compared to canonical models for the *EHB* band. The programme stars populate the EHB band between the zero-age (ZAEHB) and the terminal-age EHB (TAEHB). Most of the hottest stars (>33 000 K) are located above the TAEHB and probably have evolved off the EHB already.

6. Projected rotational velocities

With the gravity at hand, we can derive masses once the projected rotational velocities have been measured. This is not an easy task because the sdB stars are known to be slow rotators. Hence, the broad Balmer and helium lines are ill-suited.

Sharp metal lines are most sensitive to rotational broadening, in particular for low velocities, while they tend to be ironed out for fast rotators. In order to reach the best accuracy it is necessary to make use of as many weak metal lines as possible.

6.1. Projected rotational velocities from metal lines

In order to derive $v_{\rm rot} \sin i$, we compared the observed spectra with rotationally broadened, synthetic line profiles using a semi-automatic analysis pipeline. The profiles were computed for the stellar parameters given in Table 1 using the LINFOR program (developed by Holweger, Steffen and Steenbock at Kiel university, modified by Lemke 1997).

For a standard set of up to 187 unblended metal lines from 24 different ions and with wavelengths ranging from 3700 to 6000 Å a model grid with appropriate atmospheric parameters
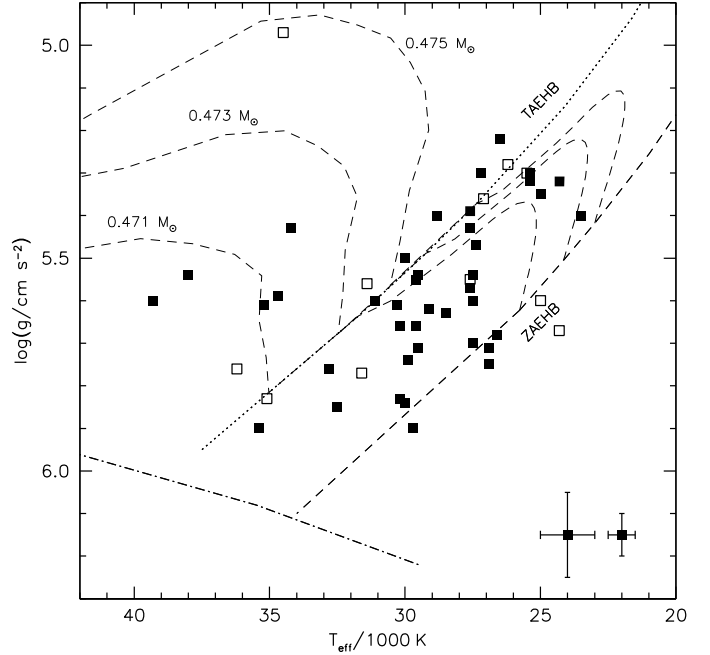

Fig. 2. $T_{\rm eff} - \log g$-diagram for the entire sample under study. The helium main sequence (HeMS) and the EHB band (limited by the zero-age EHB, ZAEHB, and the terminal-age EHB, TAEHB) are superimposed with EHB evolutionary tracks for solar metallicity taken from Dorman et al. (1993) labelled with their masses. Average error bars ($\Delta T_{\rm eff} = 500-1000$ K, $\Delta \log g = 0.05-0.10$) are given in the lower right corner. The filled symbols mark binaries with known orbital parameters (see Table 1), the open symbols radial velocity variable systems for which orbital parameters are unavailable or uncertain (see Table 3).

and different elemental abundances was automatically generated with LINFOR. The actual number of lines used as input for an individual star depended on the wavelength coverage. Due to the insufficient quality of the spectra and the pollution with telluric features in the regions blueward of 3700 Å and redward of 6000 Å we excluded them from our analysis. A simultaneous fit of elemental abundance, projected rotational velocity and radial velocity was then performed separately for every identified line using the FITSB2 routine (Napiwotzki et al. 2004b). A more detailed description of the line selection and abundance determination will be published in Paper III of this series (Geier et al., in prep.).

Ill-suited lines were rejected. This rejection procedure included several criteria. First the fitted radial velocity had to be low, because all spectra were corrected to zero RV before. Features with high RVs (>15 km s^{-1}) were considered as misidentifications or noise features. Then the fit quality given by the χ^2 had to be comparable to the average. Lines with χ^2-values more than 50% higher than the average were excluded. A spectral line was also rejected, if the elemental abundance was lower or higher than the model grid allowed. Equivalent width and depth of the line were measured and compared to the noise to distinguish between lines and noise features. Mean value and statistical error were calculated from all measurements (see Figs. 4, 5). The set of usable lines differs from star to star due to the different atmospheric parameters and chemical compositions. In some cases the line list had to be modified and lines were included or excluded after visual inspection. All outputs of the pipeline have been checked by visual inspection.

Behr (2003) used a similar method to measure the low $v_{\rm rot} \sin i$ of blue horizontal branch stars from high resolution

spectra. The errors given in that work are of the same order as the ones given here.

6.2. Systematic errors in the determination of the projected rotational velocity from metal lines

Since the velocities measured from the metal lines are low, a thorough analysis of the errors is crucial. To quantify them, we carried out numerical simulations. Synthetic spectra with fixed rotational broadening were computed and convolved with the instrumental profile. The standard list of metal lines and average sdB parameters ($T_{\rm eff} = 30\,000$ K, $\log g = 5.50$) were adopted. Random noise was added to mimic the observed spectra. The rotational broadening was measured in the way described above using a grid of synthetic spectra for various rotational broadenings and noise levels. As the resolution is seeing dependent for a subset of spectra we also varied the instrumental profile.

Variations in the instrumental profile changed the measured $v_{\rm rot} \sin i$ by up to 1.0 km s^{-1} for low S/N and poor seeing and about 0.5 km s^{-1} in case of high S/N and good seeing. The noise level caused errors ranging from 2−6 km s^{-1} per line dependent of S/N. Accounting for the number of lines used the error of the average is of the order of typically 0.5−3.0 km s^{-1}. A variation of the atmospheric parameters within the derived error limits gives an error of 0.2 km s^{-1} and is therefore negligible.

We used a standard limb darkening law for the rotational broadening independent of wavelength. Berger et al. (2005) estimated the influence of applying a wavelength dependent limb darkening law on the measurements of projected rotational velocities in DAZ white dwarf spectra. In the case of the Ca II K lines they used, a small difference in the line cores was found. Nevertheless, the systematic deviation in $v_{\rm rot} \sin i$ was smaller than 1 km s^{-1}. Because systematic errors caused by this effect would lead to higher real projected rotational velocities than measured, the influence of a wavelength dependent limb darkening law on our results was tested as well. We found the effect to be even lower, because the analysed metal lines are much weaker than the Ca II K lines used by Berger et al. (2005) and the effect becomes more significant for stronger lines. A limb darkening law independent of wavelength is therefore appropriate for our analysis.

6.2.1. Individual line fits

Our numerical experiments included typical numbers of spectral lines (20−50) as have been used in the analysis spread over the entire wavelength range available ($\simeq 3700$−6000 Å dependent on the instruments used). Figure 3 shows the results of two numerical simulations. The top panel displays the result for $v_{\rm rot} \sin i = 10$ km s^{-1} well above the detection limit and high $S/N = 100$. The fitted $v_{\rm rot} \sin i$ values for individual lines show small dispersion.

The bottom panel of Fig. 3 shows the result for $v_{\rm rot} \sin i = 7$ km s^{-1}, which is closer to the detection limit, and low $S/N = 20$. Due to the lower S/N individual lines scatter more strongly around the mean. Since negative values of $v_{\rm rot} \sin i$ are not possible, the distribution of the measurements is expected to be a truncated Gaussian. As can be seen in the lower right hand panel the distribution doesn't look like a Gaussian, but rather bimodal with many zero measurements. This distribution can be explained, because the truncation of the Gaussian occurs at the detection limit rather than $v_{\rm rot} \sin i = 0$ km s^{-1}. This detection limit is different for each star. It is caused by the thermal broadening of the lines,

which scales with $\sqrt{T_{\rm eff}/A}$, A being the atomic weight. The mix of spectral lines used ranges from C ($A = 12$) to Fe ($A = 56$). The hotter the star, the poorer the result as the number of lines decreases with $T_{\rm eff}$ while the detection limit increases. Other important parameters affecting the detection limit are spectral resolution and the S/N level of the spectra.

That is why including the zero values of the bimodal distribution in the calculation of the mean would lead to a systematic shift of $v_{\rm rot} \sin i$ to lower values (see Fig. 3 lower left panel). For this reason all zero values were excluded and the artificial rotational broadening could be measured properly. As the lower limit for this method we derived about $v_{\rm rot} \sin i > 5.0$−8.0 km s^{-1} depending on the resolution of the instrument. If more than two thirds of the lines were measured to be zero, this value was adopted as upper limit for $v_{\rm rot} \sin i$.

As can be seen in the upper panel of Fig. 3 the measured mean value slightly deviates from the true rotational broadening by 0.8 km s^{-1}. Although this deviation is still within the error bars, it turned out that such shifts of up to 1 km s^{-1} can be caused by systematic effects. The most likely explanation is that for each individual line not only the rotational broadening, but also the elemental abundance is fitted. This should affect the $v_{\rm rot} \sin i$-distribution and cause a deviation from the ideal case of random distribution around the mean. Instead of changing the rotational broadening a slightly different elemental abundance may lead to a similar χ^2-value. Due to this systematic effect a minimum $v_{\rm rot} \sin i$-error of 1.0 km s^{-1} is adopted even if the statistical error is lower.

Our analysis revealed that the restriction to just a few metal lines in a small wavelength range can lead to even higher systematic deviations and that it is better to use as many lines as possible scattered over an extended wavelength range to measure projected rotational velocities.

There is also an upper limit. With increasing $v_{\rm rot} \sin i$ the lines are getting broader and broader and eventually cannot be detected any more in spectra with S/N typical for our sample. As soon as $v_{\rm rot} \sin i$ exceeds about 25 km s^{-1} almost no metal lines can be used unless the S/N is much higher than the average of our sample. To measure higher projected rotational velocities the Balmer and helium lines must be used as described in Sect. 6.3.

6.2.2. Fitting several lines simultaneously

The FITSB2 routine also allows to fit a lot of lines simultaneously and to use different methods of calculating the fitting error (e.g. bootstrapping). In principle it is possible to measure the rotational broadening from all lines simultaneously and derive the error. But in practice this approach is problematic. Fitting up to 25 parameters (24 abundances and $v_{\rm rot} \sin i$) to more than 50 lines simultaneously and derive the error using a bootstrapping algorithm requires a lot of computer power. In test calculations we fitted up to nine lines of a synthetic spectrum with noise, rotational and instrumental broadening added simultaneously. The bootstrap error was consistent with the error we derived with the method described above. Furthermore our error estimate turned out to be slightly higher, which renders our approach more conservative. In the case of very low $v_{\rm rot} \sin i$ only some lines remain sensitive to changes in line shape due to rotational broadening. The lower limit that can be reached with the simultaneous approach is therefore higher than what can be detected with the single line approach.
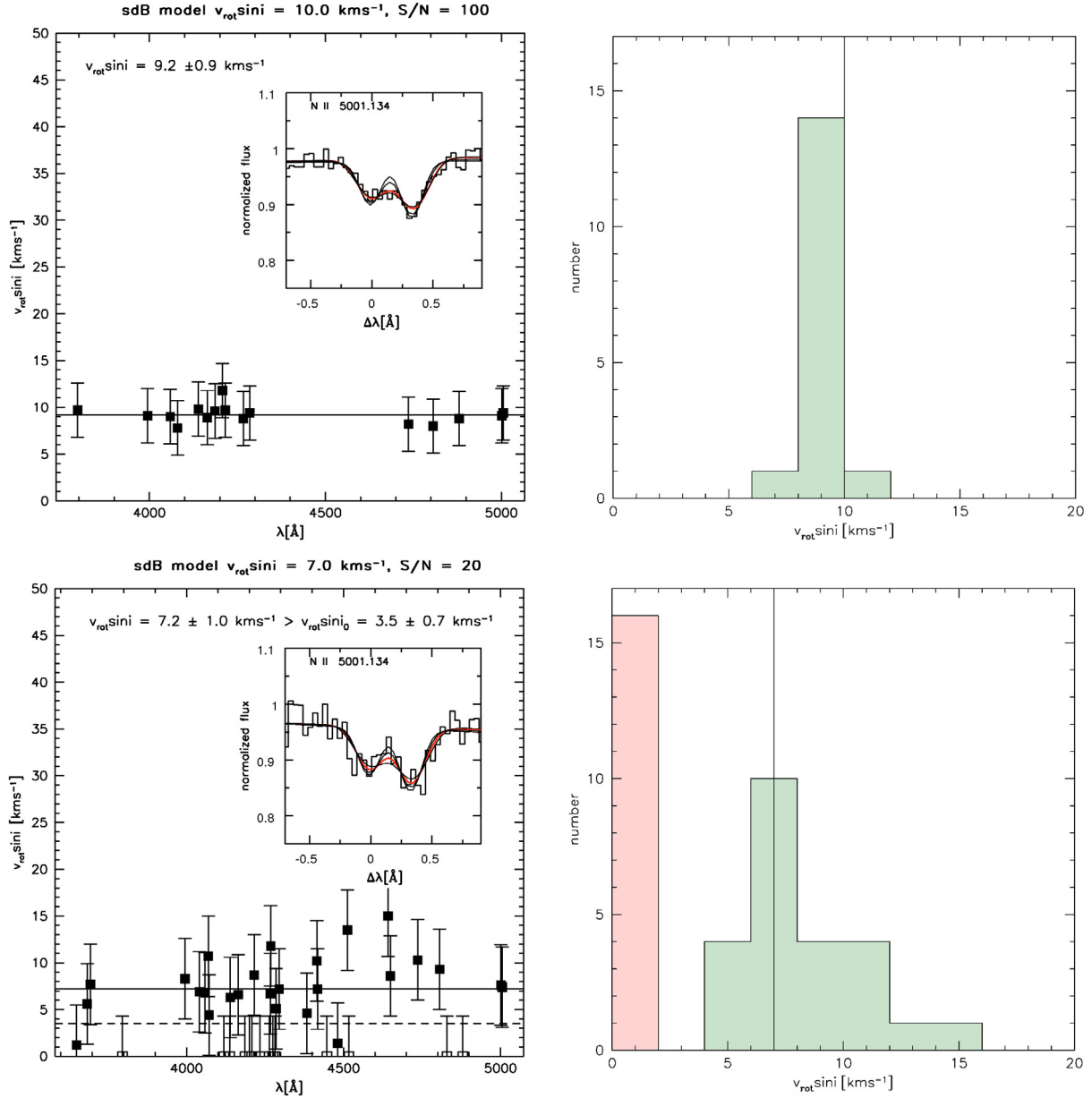
Fig. 3. *Left hand panels*: numerical simulations. $v_{rot} \sin i$ values derived from individual lines are plotted against the wavelength. Standard sdB model spectra with noise, instrumental and rotational broadening were used for the calculations. Case A (*upper left panel*): $v_{rot} \sin i = 10.0$ km s^{-1} and $S/N = 100$. The result 9.2 ± 0.9 km s^{-1} is consistent with the true value within the error margin. The distribution of individual $v_{rot} \sin i$-measurements is shown in the upper right panel. Case B (*lower left panel*): $v_{rot} \sin i = 7.0$ km s^{-1} and $S/N = 20$. Note that many lines indicate zero velocity (empty squares). The dashed line corresponds to the average including the zero values of 3.5 km s^{-1}, which is systematically lower than the true value. The zero values have to be rejected in order to obtain the result (solid line): 7.2 ± 1.0 km s^{-1} which is consistent with the true value within the error margin. *Right hand panels*: distribution of individual $v_{rot} \sin i$-measurements. The shaded bin to the left marks the zero values which have to be rejected.

6.2.3. Orbital smearing

In the case of binary systems with very short orbital periods (0.1−0.2 d) and high RV amplitudes, the variable Doppler shift of the spectral lines during the exposure can lead to a smearing effect, which can be misinterpreted as rotational broadening unless the S/N of the spectra is very high. Orbital smearing is clearly visible in most FEROS spectra of PG 1232−136, which has an orbital period of 0.36 d and an RV-semiamplitude of 130 km s^{-1} (Edelmann et al. 2005). The exposure times of these spectra ranged from 6 to 30 min. Choosing one single FEROS spectrum with sharp lines obtained at the orbital phase

when smearing should be minimal, we derived $v_{rot} \sin i = 6.2 \pm 0.8$ km s^{-1} (Geier et al. 2009a). Due to the importance of this object for our conclusions we obtained another 60 spectra of PG 1232−136 with UVES at higher resolution ($R = 80\,000$). The exposure time of each spectrum was only 2 min. After co-adding all these spectra we constrained $v_{rot} \sin i < 5.0$ km s^{-1} (see Fig. 5). Although the difference between these two results appears to be not very large, it nevertheless illustrates the influence of orbital smearing.

In the case of the short period (<0.1 d) eclipsing sdB+M binary HS 0705+6700 with an RV-semiamplitude of 86 km s^{-1} the effect is much stronger. While Drechsel et al. (2001) measure
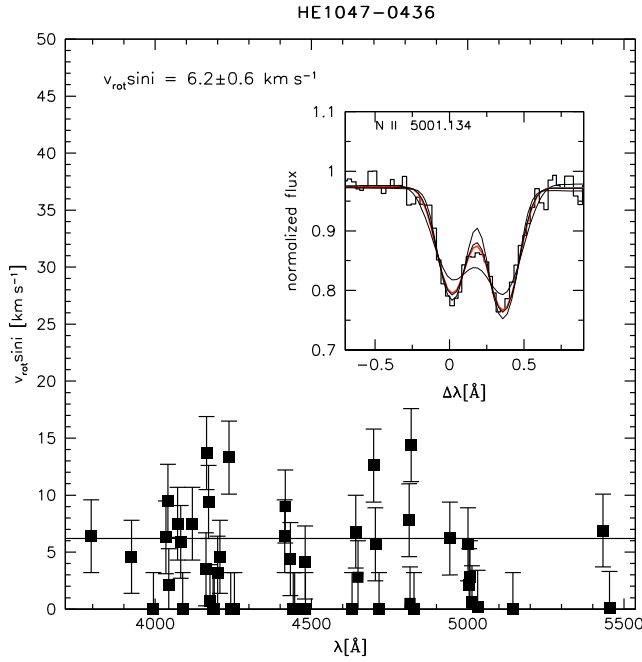
Fig. 4. Rotational broadening fit result for HE 1047−0436. The measured $v_{rot} \sin i$ is plotted against the wavelength of the analysed lines. The solid line corresponds to the average. The inlet shows an example fit of a line doublet. The thick solid line is the best fit $v_{rot} \sin i$. The three thin lines correspond to fixed rotational broadenings of $0, 5, 10$ km s^{-1}.
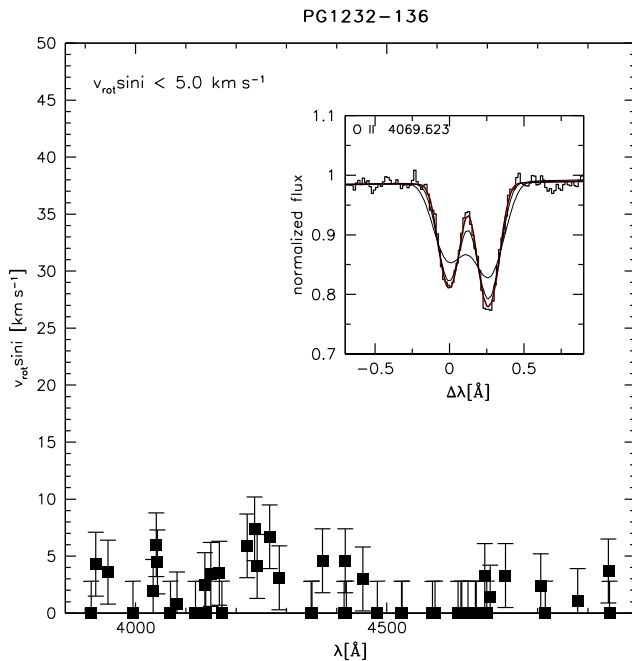

Fig. 5. Rotational broadening fit result for PG 1232−136 (see Fig. 4). Despite the high quality of the data no significant $v_{rot} \sin i$ could be measured and only an upper limit could be derived.

$v_{rot} \sin i = 110 \pm 14$ km s^{-1} from medium resolution spectra with short exposure times (10−15 min), we measure $v_{rot} \sin i = 158 \pm 12$ km s^{-1} from a high resolution spectrum taken with HET/HRS and an exposure time of 30 min. From the high resolution data we can only constrain an upper limit of $v_{rot} \sin i < 170$ km s^{-1}.

Two other stars of our sample (PG 1336−018 and PG 1043+460) may also be affected by orbital smearing, if the spectra we used were obtained during unfavourable orbital phases. Only upper limits can be given for their $v_{rot} \sin i$.

6.2.4. Other systematic errors and their impact on the companion mass determination

Other possible sources of systematic errors are broadening through microturbulence or unresolved pulsations. No significant microturbulence could be measured which is consistent with the analysis of Edelmann et al. (2001). Our sample contains six long-period pulsating sdBs of V 1093 Her type (Green et al. 2003) and four short period pulsators of V 361 Hya type (Kilkenny et al. 1997). It has been shown by Telting et al. (2008) that unresolved high amplitude pulsations with short periods can significantly contribute to or even dominate the line broadening. This is not a problem for our sample stars, because the pulsation periods of the V 1093 Her stars are long compared to our exposures times and the amplitudes are low. No significant pulsational broadening is expected in the case of the short period pulsators Feige 48 and HE 0230−4323 as well, because the amplitudes of the pulsations are low (Reed et al. 2004; Charpinet et al. 2005b; Kilkenny et al. 2010). The line broadening of KPD 1930+2752 and PG 1336−018 is totally dominated by their rotation, because the sdBs are spun up by their close companions (Geier et al. 2007; Vučković et al. 2007).

It has to be pointed out that unresolved pulsations, microturbulence and any other unconsidered effect would cause an extra broadening of the lines. The true projected rotational velocity would therefore always be lower than the one we determined. In this case the derived orbital inclination would also be lower and the estimated mass of the unseen companion would be higher (see Sect. 4). Unaccounted systematic effects would therefore lead to higher companion masses. This fact is important for the interpretation of the results (see Sect. 7).

6.3. Projected rotational velocities from hydrogen and helium lines

A few sdBs, which reside in close binary systems, are known to be spun up by the tidal influence of their companions. The projected rotational velocities of these stars are as high as 100 km s^{-1} (e.g. Drechsel et al. 2001; Geier et al. 2007).

Rotational broadening irons out the weak metal lines unless the spectra are of excellent S/N. However, for higher projected rotational velocities, Balmer and helium lines remain the only choice to determine $v_{rot} \sin i$. Due to thermal and pressure broadening Balmer and helium lines are less sensitive to rotational broadening than metal lines. From our simulations we derive detection limits of $v_{rot} \sin i \simeq 15$ km s^{-1} for helium lines and $v_{rot} \sin i \simeq 25$ km s^{-1} for the Balmer line cores given an $S/N \simeq 100$. For lower quality data these limits go up significantly. For many of our spectra the Balmer and helium lines are insensitive unless $v_{rot} \sin i$ exceeds $\simeq 50$ km s^{-1}.

To measure the $v_{rot} \sin i$ we calculated LTE model spectra with the appropriate atmospheric parameters (see Table 1) and performed a simultaneous fit of rotational broadening and helium abundance to all usable Balmer line cores and helium lines using the FITSB2 routine (Napiwotzki et al. 2004b, for an example see Fig. 7). All systematic effects discussed in the previous section except orbital smearing become negligible in this case. The quoted uncertainties are 1σ-χ^2-fit errors.
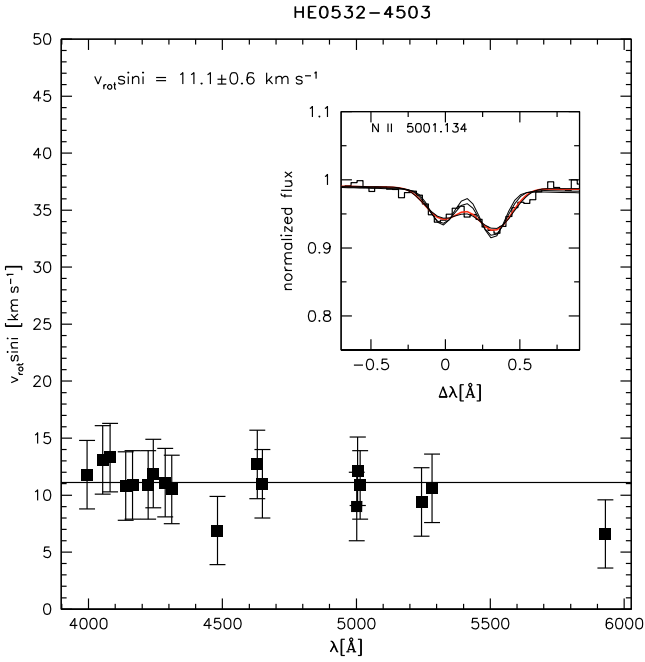
Fig. 6. Rotational broadening fit result for HE 0532−4503 (see Fig. 4).
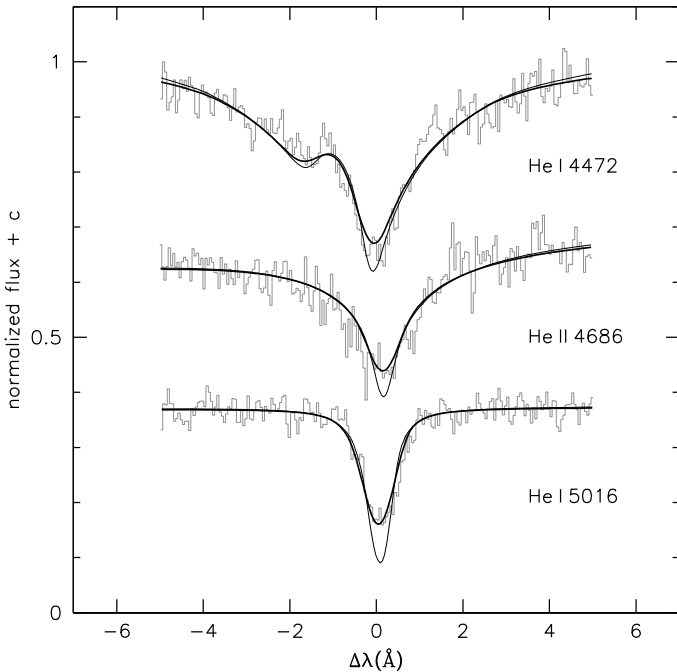

Fig. 7. Selected helium lines of KPD 1946+4340 are plotted against the shift relative to rest wavelengths. The spectrum (histogram) is overplotted with the best fitting rotationally broadened model (strong line). A model without rotational broadening (weak line) is overplotted for comparison.

The helium ionisation problem in hot sdBs (see Sect. 5) caused by neglected metal opacity can affect the measurement of the rotational broadening, if helium lines are used. This became apparent in the analysis of the eclipsing sdOB binary AA Dor. While Rauch & Werner (2003) used metal-free NLTE models and measured $v_{rot} \sin i = 47 \pm 5$ km s^{-1} for the He II line at 4686 Å, Fleig et al. (2008) measured $v_{rot} \sin i = 35 \pm 5$ km s^{-1}

by fitting metal line blanketed NLTE models to FUSE spectra. Rucinski (2009) derived $v_{rot} \sin i$ by an analysis of line profile variations during the eclipse and reported a mismatch between the Mg II line at 4481 Å and the He II line at 4686 Å. Müller et al. (2010) resolved this conundrum and showed that consistent results ($v_{rot} \sin i = 30 \pm 1$ km s^{-1}) can be achieved if the appropriate (metal enriched) model atmospheres are used (see Sect. 5).

To account for this effect we used LTE models with ten times solar metallicity rather than metal-free NLTE models to measure the rotational broadening of the Balmer line cores and helium lines in the two hot sdOBs KPD 1946+4340 (see Fig. 7) and [CW83] 1735+22. While in the case of [CW83] 1735+22 the $v_{rot} \sin i$-values derived with the two different model grids were the same, a significant difference was measured for KPD 1946+4340. The $v_{rot} \sin i$ derived with the metal-free models was 42 km s^{-1} compared to 26 km s^{-1} with metal-enriched models.

Due to the fact that KPD 1946+4340 is eclipsing (Bloemen et al. 2010) it is possible to verify that the $v_{rot} \sin i$ measured with metal enriched models is fully consistent with the assumption of synchronised rotation (see Sect. 10).

6.4. Results

Projected rotational velocities of 46 close binary subdwarfs have been measured and supplemented by five measurements taken from literature (Tables 2 and 3). For 40 systems the orbital parameters are known. In general the projected rotational velocities are small. The other 11 systems are slow rotators, too. These systems can not be analysed further as their mass functions are still unknown.

The projected rotational velocities of HE 1047−0436 and Feige 48 have been measured by Napiwotzki et al. (2001a) and O'Toole et al. (2004) using a technique similar to the one described here, but restricted to just a few metal lines. Napiwotzki et al. (2001a) derived an upper limit of $v_{rot} \sin i = 4.7$ km s^{-1} for HE 1047−0436. Our measurement of 6.2 ± 0.6 km s^{-1} is just slightly higher (see Fig. 4). While O'Toole et al. (2004) give an upper limit of $v_{rot} \sin i = 5$ km s^{-1} for Feige 48 we derive 8.5 ± 1.5 km s^{-1}.

Figure 9 shows the measured $v_{rot} \sin i$ plotted against the orbital periods of the binaries. A trend is clearly visible: The longer the orbital period of the systems, the lower the measured $v_{rot} \sin i$. While the short period systems ($\simeq 0.1$ d) were spun up by their close companions and have high $v_{rot} \sin i$ up to $\simeq 100$ km s^{-1}, the mean $v_{rot} \sin i$ decrease to below 10 km s^{-1} as the periods increase to $\simeq 1.0$ d. For orbital periods exceeding $\simeq 1.0$ d, the $v_{rot} \sin i$-values scatter around the average $v_{rot} = 8.3$ km s^{-1} for single sdB stars (Geier et al. 2009a). We conclude that tidal forces do not influence the rotation of sdBs for orbital periods considerably longer than one day.

As can be seen in Fig. 8 the $v_{rot} \sin i$-distribution of the RV variable sdBs (Tables 2, 3) differs from the uniform distribution of the single stars (Geier et al. 2009a). The rotational properties of the full sample of single sdB stars will be presented in paper II of this series by Geier et al. (in prep.). A large fraction of binary sdBs exceeds the derived maximum $v_{rot} = 8.3$ km s^{-1} significantly. The most likely reason for this is tidal interaction with the companions.

Table 2. Projected rotational velocities for the binary sdB systems from Table 1.

System	$T_{\rm eff}$ [K]	m_B [mag]	S/N	Seeing [arcsec]	$N_{\rm lines}$	$v_{\rm rot} \sin i$ [km s^{-1}]	Instrument	Reference
PG 1627+017[l]	23 500	11.3	64		11	<7.0	HRS	
GD 687	24 300					21.2 ± 2.0		Geier et al. (2010a)
JL 82[l]	25 000	12.2	55		57	10.4 ± 1.0	FEROS	
PB 7352	25 000	12.0	61		39	7.4 ± 1.0	FEROS	
HE 0532−4503	25 400	16.1	83	0.8	18	11.1 ± 1.0	UVES	
PG 0001+275[l]	25 400	12.8	129		24	12.6 ± 1.0	FOCES	
PG 1248+164	26 600	14.4	47		13	8.9 ± 1.3	HRS	
PG 1232−136	26 900	13.1	167		64	<5.0	UVES	
PG 1432+159	26 900	13.6	50		22	9.5 ± 1.0	HRS	
PG 1716+426[l]	27 400	13.7	61		24	10.9 ± 1.0	HRS	
PG 0101+039[l]	27 500					10.9 ± 1.1		Geier et al. (2008a)
CPD −64 481	27 500	11.0	152		38	4.1 ± 1.0	FEROS	
PG 2345+318	27 500	14.4	92		21	12.9 ± 1.0	HRS	
PG 1043+760[l]	27 600	13.4	15		H/He	<88	Palomar	
PG 1743+477	27 600	13.6	57		27	<7.0	HRS	
TON S 183	27 600	12.4	55		57	6.7 ± 1.0	FEROS	
HD 171858	27 700	9.6	90		55	6.7 ± 1.0	FEROS	
HW Vir	28 500	10.3	130		H/He	78.3 ± 1.0	FEROS	
HS 0705+6700	28 800	14.2	28		H/He	<170	HRS	
					H/He	110 ± 14		Drechsel et al. (2001)
PG 1329+159	29 100	13.3	52		26	10.7 ± 1.0	HRS	
Feige 48[s]	29 500	13.1	37		36	8.5 ± 1.0	HIRES	
HE 0929−0424	29 500	15.4	25	0.6	9	7.1 ± 1.0	UVES	
HE 1421−1206	29 600	15.1	21	0.5	18	6.7 ± 1.1	UVES	
PG 0133+114	29 600	10.7	194		17	<8.0	FOCES	
PG 1101+249	29 700	12.5	66		24	8.1 ± 1.0	HIRES	
PG 1512+244	29 900	13.0	87		17	<8.0	HRS	
HE 2135−3749	30 000	13.7	84	1.0	53	6.9 ± 1.0	UVES	
PHL 861	30 000	15.1	24	0.6	16	7.2 ± 1.3	UVES	
HE 1047−0436	30 200	14.7	37	0.6	37	6.2 ± 1.0	UVES	
HE 2150−0238	30 200	15.8	27	0.8	16	8.3 ± 1.5	UVES	
PG 1017+086	30 300				H/He	118 ± 5		Maxted et al. (2002)
HE 0230−4323[s]	31 100	13.8	59	0.9	40	12.7 ± 1.0	UVES	
PG 1336−018[s]	31 300	14.0	40		H/He	<79.0	FEROS	
PG 1116+301	32 500	14.3	42		8	9.0 ± 1.7	HRS	
KPD 1946+4340	34 200	14.1	55		H/He	26.0 ± 1.0	HRS	
HE 1448−0510	34 700	15.0	27	0.6	8	7.2 ± 1.7	UVES	
KPD 1930+2752[s]	35 200					92.3 ± 1.5		Geier et al. (2007)
CD −24 731	35 400	11.6	42		8	12.1 ± 1.7	FEROS	
[CW83] 1735+22	38 000	11.5	230		H/He	44.0 ± 1.0	FOCES	
BPS CS 22169−0001	39 300	12.6	109		5	8.5 ± 1.5	FEROS	

Notes. For binaries with high $v_{\rm rot} \sin i$ helium lines and Balmer line cores (H/He) are used instead of metal lines. The average seeing is only given if the spectra were obtained with a wide slit in the course of the SPY survey. In all other cases the seeing should not influence the measurements. [c] Companion visible in the spectrum. [s] Pulsating subdwarf of V 361 Hya type. [l] Pulsating subdwarf of V 1093 Her type.

Table 3. Projected rotational velocities of radial velocity variable sdBs, for which orbital parameters are unavailable or uncertain.

System	$T_{\rm eff}$ [K]	m_B [mag]	S/N	seeing [arcsec]	$N_{\rm lines}$	$v_{\rm rot} \sin i$ [km s^{-1}]	Instrument
HE 2208+0126	24 300	15.6	24	0.8	15	<5.0	UVES
TON S 135	25 000	13.1	47		35	6.6 ± 1.0	FEROS
HE 2322−4559[c]	25 500	15.5	23	0.7	16	10.9 ± 1.1	UVES
HS 2043+0615	26 200	16.0	22	1.3	26	12.3 ± 1.1	UVES
HE 1309−1102[c]	27 100	16.1	7	0.6	7	7.6 ± 2.3	UVES
HS 2357+2201	27 600	13.3	29	0.7	26	6.1 ± 1.1	UVES
HS 2359+1942	31 400	14.4	14	0.6	26	< 5.0	UVES
PG 1032+406	31 600	10.8	20		H/He	<34	Palomar
HE 1140−0500[c]	34 500	14.8	18	0.9	5	5.2 ± 2.7	UVES
HS 1536+0944[c]	35 100	15.6	19	1.1	15	12.2 ± 1.6	UVES
HE 1033−2353	36 200	16.0	13	0.6	7	9.3 ± 2.3	UVES

Notes. The average seeing is only given if the spectra were obtained with a wide slit in the course of the SPY survey. In all other cases the seeing should not influence the measurements. Atmospheric parameters are taken from Lisker et al. (2005) except TON S 135 (Heber 1986) and PG 1032+406 (Maxted et al. 2001). [c] Companion visible in the spectrum.
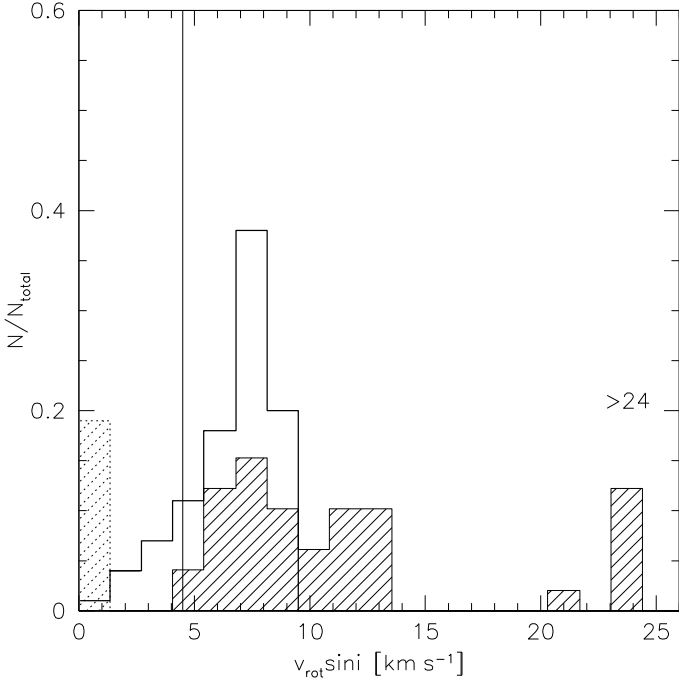
Fig. 8. Shaded histogram showing the distribution of the measured $v_{\rm rot} \sin i$ of 51 RV variable sdBs. The blank histogram marks the expected uniform distribution of $v_{\rm rot} \sin i$, if the rotational velocity were the same for all stars ($v_{\rm rot} = 8.3$ km s^{-1}) and rotation axes were randomly oriented. The solid vertical line at $v_{\rm rot} \sin i \simeq 5.0$ km s^{-1} marks the detection limit. All sdBs with lower $v_{\rm rot} \sin i$ are stacked into the first bin (dotted histogram). All sdBs with $v_{\rm rot} \sin i$ higher than 24 km s^{-1} are summed up in the last bin.
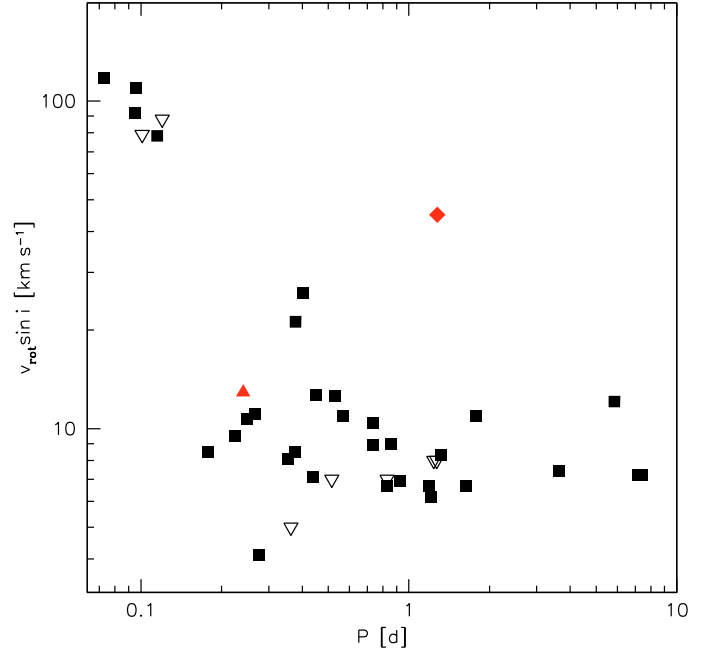

Fig. 9. The measured $v_{\rm rot} \sin i$ of 40 RV variable sdBs plotted against the orbital period of the binaries (Tables 2, 1). For seven stars, marked as open inverted triangles, only upper limits were derived. The solid diamond marks [CW83] 1735+22 that rotates faster than synchronised (see Sect. 11.1 for a detailed discussion). PG 2345+318 rotates slower than synchronised and is marked with a filled triangle (see Sect. 11.2 for a discussion).

7. Constraining masses, inclinations and the nature of the unseen companions

Having determined the projected rotational velocity we are in a position to derive the companion mass as a function of the sdB mass as described in Sect. 4.

From 40 sdB binaries, for which all necessary parameters have been determined, 31 could be solved consistently under the assumption of tidally locked rotation. Two examples are shown in Figs. 10 and 11. Derived inclinations, subdwarf masses and the allowed masses for the companions are given in Table 4.

If the sdB mass could not be constrained with other methods (e.g. from photometry, see Table 4), the theoretically predicted mass range was taken from Han et al. (2002, 2003). For the common envelope ejection channels, which are the only plausible way of forming sdBs in close binary systems, the possible masses for the sdBs range from 0.38 $M_\odot$ to 0.47 $M_\odot$. Since in all simulation sets of Han et al. (2002, 2003) the mass distribution shows a very prominent peak at 0.43−0.47 $M_\odot$ this mass range is the most likely one.

The choice of the adopted sdB mass range is backed up by recent mass determinations via asteroseismology of short-period pulsating sdBs. Fontaine et al. (2008) showed the mass distribution of 12 of these objects, which is in good agreement with the predicted distribution by Han et al. (2002, 2003). Consistent with theory no star of this small sample has a mass much lower than 0.4 $M_\odot$. The few sdB masses, that could be constrained by analyses of eclipsing binary systems also range from 0.38 $M_\odot$ to 0.5 $M_\odot$ (see e.g. Sect. 7.1 and For et al. 2010).

Hence we adopt 0.43 − 0.47 $M_\odot$ as the mass range for the sdBs in the binary systems we studied, if there is no independent mass determination either from binary light curve analysis or asteroseismology.

If the derived minimum sdB mass assuming a sychronised orbit (see Eq. (4)) exceeds this reasonable mass range ($M_{\rm sdB} \gg 1 \, M_\odot$) the sdB primary spins faster than synchronised and no consistent solution can be found. This is the case for 9 binaries from our sample. Most of these systems have orbital periods exceeding 1.2 d, where we find that synchronisation is no longer established (see Sect. 9). It has to be pointed out that only subdwarfs rotating faster than synchronised can be identified in this way. If an sdB should rotate slower than synchronised, one would always get an apparently consistent, but incorrect solution, which overestimates the companion mass (see Sect. 11.2). For **PG 0133+114** there is some doubt whether the star is synchronised or not as the minimum mass for the sdB is 0.51 $M_\odot$ at the upper end of the predicted mass range for core helium-burning objects and its period is rather long (1.24 d). The minimum companion mass would be 0.38 $M_\odot$, while the statistically most likely one ($i = 52°$) 0.48 $M_\odot$, indicating it is a white dwarf, if the system is synchronised.

The nature of the companion was deduced unambiguously for most of the remaining stars (except five) from the masses and additional information. The companions to **PG 1248+164**[2], **HE 1421−1206**, **Feige 48**[3], and **HE 2135−3749** could be either

---

[2] A light curve of this star has been taken by Maxted et al. (2004). No variability could be detected. Although the orbital period is rather long (0.73 d) and a reflection effect therefore shallow, the companion may be a low-mass WD rather than an M dwarf.

[3] The mass of the pulsating subdwarf Feige 48 has been determined in an asteroseismic analysis (van Grootel et al. 2008) to 0.52 $M_\odot$. The corresponding companion mass is 0.27 $M_\odot$. Therefore the nature of the unseen companion remains unclear. It may be a low mass white dwarf as well as a late M dwarf. Due to the derived very low inclination and

main sequence stars or white dwarfs because their masses are lower than 0.45 $M_\odot$.

We shall describe the results for three groups of companion stars. Starting with sdBs orbited by low mass dwarf companions, we proceed to the systems with white dwarf companions of normal masses. Finally we discuss the group of binaries that contain massive compact companions exceeding 0.9 $M_\odot$, because such systems are of particular interest, e.g. as potential SN Ia progenitors. This includes KPD 1930+2752, the most massive white dwarf companion to an sdB star known so far.

7.1. Late main sequence stars and a potential brown dwarf

PG 1017−086 is the sdB binary with the shortest orbital period known to date. Maxted et al. (2002) reported the detection of a significant reflection effect, but no eclipses in the light curve. Taking these informations into account, one can constrain the inclination angle to be lower than 73° (no eclipses!) and derive a minimum sdB mass of 0.47 $M_\odot$. The minimum mass of the companion is constrained to 0.06 $M_\odot$. The companion is therefore most likely a brown dwarf (BD) or a very late M dwarf. Only two other candidate sdB+BD systems are known.

HS 0705+6700 is an eclipsing sdB+M binary with reflection effect. Drechsel et al. (2001) performed a detailed photometric and spectroscopic analysis of this system and derived an inclination of 84°.4, an sdB mass of 0.483 $M_\odot$ and a companion mass of 0.134 $M_\odot$. Drechsel et al. (2001) also estimated $v_{rot} \sin i$ and derived the companion mass. Although our result is much less accurate ($0.15^{+0.05}_{-0.03}$ $M_\odot$), it comes close to that derived from the light curve.

Much better agreement is reached for **HW Vir**, the prototype eclipsing sdB+M binary, where excellent high resolution spectra are available. Edelmann (2008) recently determined the absolute parameters of this system spectroscopically using shallow absorption lines of the secondary to obtain its RV curve for the first time[4]. Edelmann (2008) derives an sdB mass of 0.53 $M_\odot$ and a companion mass of 0.15 $M_\odot$. Adopting this sdB mass our derivation of the companion mass agrees very well ($0.155^{+0.015}_{-0.015}$ $M_\odot$). The derived inclination angle of $i = 75^{+15}_{-10}$° is consistent with the more accurate photometric solution $i = 80°.6 \pm 0°.2$ given by Wood et al. (1993). Most recently Lee et al. (2009) presented an analysis on HW Vir based on new photometric data. Their best solution ($i = 80°.98 \pm 0°.1$, $M_1 = 0.485 \pm 0.013$ $M_\odot$, $M_2 = 0.142 \pm 0.004$ $M_\odot$) is fully consistent with our results.

The eclipsing and pulsating sdBV+M binary **PG 1336−018** (NY Vir) has been analysed by Vučković et al. (2008), but no unique solution could be found. In an asteroseismic study Charpinet et al. (2008) derived the fundamental parameters of this star by fitting simultaneously the observed pulsation modes detectable in the light curve. Adopting the asteroseismic value for the sdB mass (0.459 $M_\odot$) for our analysis, the companion mass is >0.12 $M_\odot$. This result is in agreement with the second solution from Vučković et al. (2008): $M_{sdB} = 0.467$ $M_\odot$, $M_{comp} = 0.122$ $M_\odot$. Charpinet et al. (2008) concluded that the binary must be synchronised to account for the observed rotational splitting of the pulsation modes and predict a $v_{rot} \sin i = 74.9 \pm 0.6$ km s^{-1}. This predicted value is consistent with the derived upper limit of $v_{rot} \sin i < 79$ km s^{-1}.

---

the presence of short period pulsations, a reflection effect or ellipsoidal variations are probably too small to be detectable.

[4] Wood & Saffer (1999) detected these features in low resolution spectra before.

BPS CS 22169−0001 was proposed to host a BD companion (Edelmann et al. 2005), but we derived a very low inclination and therefore a companion mass too high for a BD ($0.19^{+0.07}_{-0.06}$ $M_\odot$). In the light curves of the four binaries **BPS CS 22169−0001**, **HE 0230−4323**, **JL 82** as well as **PG 1329+159** reflection effects have been detected (see references in Table 4). The derived companion mass ranges are consistent with the masses of late M dwarfs.

7.2. White dwarfs

Ten stars must have white dwarf companions because no lines from cool companions are visible and the absence of a reflection effect can be used to exclude a main sequence companion in some cases.

Among these binaries **KPD 1946+4340** sticks out. Most recently Bloemen et al. (2010) discovered eclipses and ellipsoidal variations in a spectacular high precision light curve obtained by the Kepler mission. The eclipses are clearly caused by a WD companion. We derive a mass range of 0.59−0.85 $M_\odot$ for the unseen companion consistent with a WD. Due to the fact that the binary is eclipsing, the inclination angle has to be close to 90°. Assuming the canonical sdB mass of 0.47 $M_\odot$ the companion mass can be constrained to ≃0.61 $M_\odot$, which is the average mass of WDs with C/O core. This result is perfectly consistent with the indepedent analysis of Bloemen et al. (2010).

The companion of **GD 687** has already been shown to be a white dwarf by Geier et al. (2010a) utilising the same technique as used in this paper and is included for the sake of completeness. Its merging time is 11.1 Gyr, which is just a little shorter than the Hubble time[5].

A remarkable object which has a high inclination and a very low companion mass (>0.10 $M_\odot$) is **PG 1043+760**. Due to its short period of 0.12 d a reflection effect should be easily detectable. But Maxted et al. (2004) report a non-detection of variations in the light curve. The companion of this star must be a compact object, most likely a helium-core white dwarf of very low mass.

In the case of **PG 1627+017**, a main sequence companion can be excluded as well. With a mass exceeding 0.50 $M_\odot$ the companion would be visible in the spectra in this case. The non-detection of a reflection effect (Maxted et al. 2004; For et al. 2010) is consistent with our result.

The companion of **PG 0101+039** is a white dwarf. Despite of the long orbital period of 0.57 d a main-sequence companion could be excluded. A light curve was taken with the MOST satellite. Instead of a reflection effect the shallowest ellipsoidal deformation ever detected could be verified (Geier et al. 2008a). The white dwarf companion could be quite massive (0.52−0.92 $M_\odot$). In this case the total mass comes close the Chandrasekhar limit, but the merging time would be higher than the Hubble time. PG 0101−039 does therefore not qualify as SN Ia progenitor candidate. The companion mass range of **PG 0001+275** is quite similar (0.56−1.05 $M_\odot$). A main sequence companion can be most likely excluded and no reflection effect was detected (Maxted et al. 2004; Shimanskii et al. 2008). The orbital period of 0.53 d is also too long to make PG 0001+275 a SN Ia progenitor candidate.

Edelmann et al. (2005) derived a very low minimum companion mass for **CPD −64 481**. At high inclination the companion mass would have been consistent with a brown dwarf.

---

[5] The merging times of all binaries have been calculated using the formula given in Ergma et al. (2001).

Table 4. Derived inclination angles, companion masses and likely nature of the companions.

System	P^* [d]	M_{sdB} [$M_\odot$]	i [deg]	M_{comp} [$M_\odot$]	i_{max} [deg]	$M_{comp,min}$ [$M_\odot$]	Companion
PG 1017−086[12]	0.07	>0.47	<73	>0.06			MS/BD^r
KPD 1930+2752[6]	0.10	$0.47^{+0.05}_{-0.02}$	77^{+4}_{-4}	$0.94^{+0.02}_{-0.03}$			WD^{el}
HS 0705+6700[3]	0.10	0.48	65^{+25}_{-16}	$0.15^{+0.05}_{-0.03}$			MS^{r,ec}
PG 1336−018[2,16]	0.10	0.459	<90	>0.12			MS^r
HW Vir[4]	0.12	0.53	75^{+15}_{-10}	$0.155^{+0.015}_{-0.015}$			MS^{r,ec}
PG 1043+760[13]	0.12		<78	>0.10	90	0.06	WD^n
BPS CS 22169−0001[14]	0.18		9^{+2}_{-2}	$0.19^{+0.07}_{-0.06}$	13	0.09	MS^r
PG 1432+159[12]	0.22		16^{+5}_{-3}	$2.59^{+2.01}_{-1.10}$	25	0.92	NS/BH^n
PG 2345+318[2]	0.24						WD^{ec} not synchronised
PG 1329+159[12]	0.25		17^{+4}_{-2}	$0.35^{+0.10}_{-0.10}$	26	0.16	MS^r
HE 0532−4503[11]	0.27		14^{+2}_{-2}	$3.00^{+0.94}_{-0.92}$	19	1.27	NS/BH^f
CPD −64 481	0.28		7^{+2}_{-2}	$0.62^{+0.42}_{-0.24}$	11	0.24	WD
PG 1101+249	0.35		26^{+6}_{-4}	$1.67^{+0.77}_{-0.58}$	40	0.68	WD/NS/BH^f
PG 1232−136	0.36		<14	>6.00	17	3.58	BH^f
Feige 48[15]	0.38	0.52	17^{+3}_{-2}	$0.27^{+0.06}_{-0.04}$			MS/WD
GD 687[5,7]	0.38		39^{+6}_{-6}	$0.71^{+0.22}_{-0.21}$	63	0.32	WD^f
KPD 1946+4340[1]	0.40		71^{+19}_{-15}	$0.67^{+0.18}_{-0.08}$	90	0.58	WD^{el,ec}
HE 0929−0424[11]	0.44		23^{+5}_{-4}	$1.82^{+0.88}_{-0.64}$	34	0.73	WD/NS/BH^f
HE 0230−4323[9]	0.45		39^{+8}_{-5}	$0.30^{+0.07}_{-0.07}$	61	0.15	MS^r
PG 1743+477	0.52		<27	>1.66	32	1.00	NS/BH^f
PG 0001+275	0.53		31^{+7}_{-4}	$0.79^{+0.26}_{-0.23}$	48	0.37	WD
PG 0101+039[8]	0.57		40^{+9}_{-6}	$0.72^{+0.20}_{-0.20}$	64	0.33	WD^{el,n}
PG 1248+164	0.73		52^{+25}_{-12}	$0.27^{+0.10}_{-0.08}$	90	0.12	MS/WD
JL 82[10]	0.74		33^{+8}_{-5}	$0.21^{+0.06}_{-0.06}$	51	0.10	MS^r
TON S 183	0.83		30^{+7}_{-5}	$0.94^{+0.39}_{-0.31}$	47	0.40	WD^f
PG 1627+017	0.83		<34	>0.50	45	0.32	WD
PG 1116+301	0.86		90	$0.48^{+0.00}_{-0.21}$	90	0.27	WD
HE 2135−3749	0.92		67^{+13}_{-16}	$0.41^{+0.13}_{-0.12}$	90	0.29	MS/WD
HE 1421−1206	1.19		57^{+33}_{-14}	$0.27^{+0.10}_{-0.08}$	90	0.16	MS/WD
HE 1047−0436	1.21		62^{+28}_{-10}	$0.53^{+0.15}_{-0.14}$	90	0.28	WD
PG 0133+114	1.24	> 0.51	90	> 0.38			MS/WD/not synchronised?
PG 1512+244	1.27						not synchronised?
[CW83] 1735+22	1.28						not synchronised
HE 2150−0238	1.32						not synchronised
HD 171858	1.63		58^{+32}_{-14}	$0.60^{+0.25}_{-0.19}$	90	0.37	WD
PG 1716+426	1.78						not synchronised
PB 7352	3.62						not synchronised
CD −24 731	5.85						not synchronised
HE 1448−0510	7.16						not synchronised
PHL 861	7.44						not synchronised

Notes. If the sdB mass couldn't be constrained with other methods the theoretically predicted mass range of 0.43−0.47 $M_\odot$ was taken from Han et al. (2002, 2003). The minimum masses of the companions and maximum inclinations of the binaries were calculated for the lowest possible sdB mass (0.3 $M_\odot$, Han et al. 2002, 2003). * The orbital periods given here are rounded to the second decimal place. The accurate values are given in Table 1. Additional constraints to clarify the nature of the unseen companions: ^{r} The detection of a reflection effect from a cool MS/BD or a ^{n} non-detection to exclude this option. The presence of eclipses ^{ec} or ellipsoidal deformations ^{el} in the light curves. No signatures of a main-sequence companion within the given mass range are visible in the flux distribution or in the spectrum ^{f}. These informations are taken from [1] Bloemen et al. (2010), [2] Charpinet et al. (2008), [3] Drechsel et al. (2001), [4] Edelmann (2008), [5] Farihi et al. (2005), [6] Geier et al. (2007), [7] Geier et al. (2010a), [8] Geier et al. (2008a), [9] Koen (2007), [10] Koen (2009), [11] Lisker et al. (2005), [12] Maxted et al. (2002), [13] Maxted et al. (2004), [14] Østensen (priv. comm.), [15] van Grootel et al. (2008), and [16] Vučković et al. (2007).

However, our analysis provides evidence that this binary has a very low inclination (i = 5° to 9°), actually the lowest one of the entire sample, and therefore a companion mass way too high for a BD ($0.62^{+0.42}_{-0.24}$ $M_\odot$) indicating a white dwarf binary. Due to the low projected rotational velocity of this star, the fractional error is very high and the companion mass not very well constrained. For the highest possible companion mass the system would exceed the Chandrasekhar limit and qualify as

SN Ia progenitor candidate due to its short orbital period. However, the inclination angle must be lower than 5° is this case. That is why this extreme scenario is considered to be very unlikely.

The unseen companions in the binaries **HE 1047−0436**, and **HD 171858** also have masses consistent with white dwarfs.

The mass of the companion to **PG 1116+301** is slightly above the limit of 0.45 $M_\odot$. Despite the high inclination derived
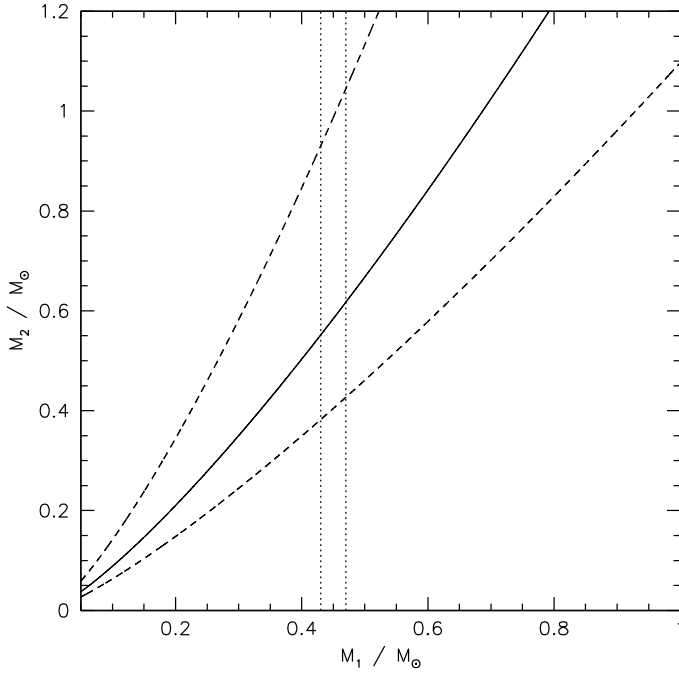
Fig. 10. Mass of the sdB primary CPD −64 481 plotted against the mass of the unseen companion. The companion mass error is indicated by the dashed lines. The mass range of the CE ejection channel (Han et al. 2002) is marked with dotted vertical lines.

for this binary no reflection effect was detected in its light curve (Maxted et al. 2004; Shimanskii et al. 2008), which is consistent with a WD companion[6].

7.3. Massive compact companions – white dwarfs, neutron stars, black holes

Seven subdwarf binaries (in addition to KPD 1930+2752) have massive compact companions (see e.g. Figure 11) exceeding 0.9 $M_\odot$. For all of these binaries main sequence companions can be excluded, because they would significantly contribute to the flux or even outshine the subdwarf primary. The massive companions therefore have to be compact.

The nature of the unseen companion in the binary **KPD 1930+2752** could be clarified by Geier et al. (2007). The short period system consists of a synchronously rotating, tidally distorted sdB and a massive white dwarf. The combined mass of the systems reaches the Chandrasekhar limit and the stars will most probably merge in 200 Myr. KPD 1930+2752 is the best double degenerate candidate for SN Ia progenitor so far.

The companion mass of **TON S 183** is as high as that of KPD 1930+2752. However, the error bar is much larger. Hence we can not exclude that it is a normal white dwarf of 0.6 $M_\odot$. On the other hand the total mass of the system may exceed the Chandrasekhar limit, but TON S 183 does also not qualify as SN Ia progenitor candidate, because of its long orbital period the merging time exceeds the Hubble time by orders of magnitude.

For **PG 1101+249** and **HE 0929−0424** the companion mass is slightly above the Chandrasekhar limit, but we can not exclude a massive white dwarf given the errors. The merging times of
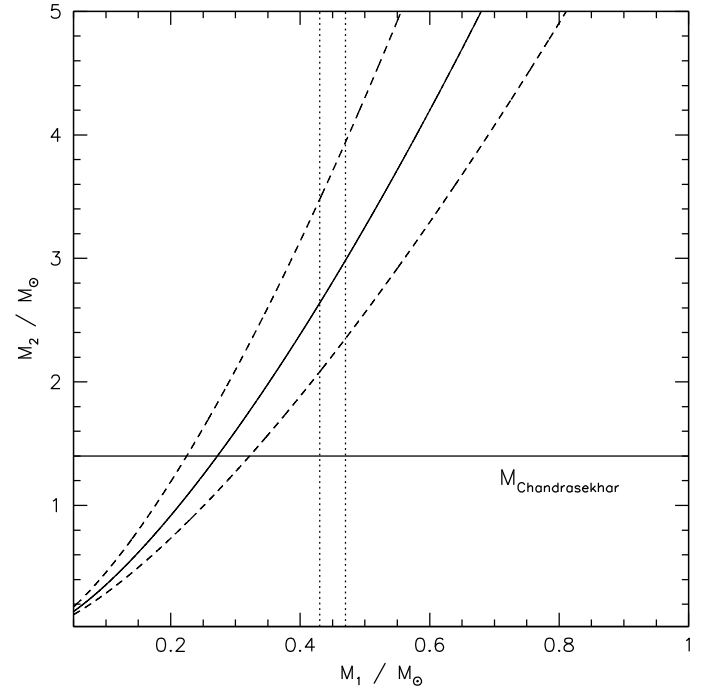
[6] The upper limit to the companion mass of PG 1116+301 is identical with the most likely companion mass (see Table 4, Fig. 14). The system can only be synchronised if the inclination reaches its maximum value of 90°. In this case the upper limit to the sdB mass is lower than 0.47 $M_\odot$, but still within the possible range (see Sect. 4).
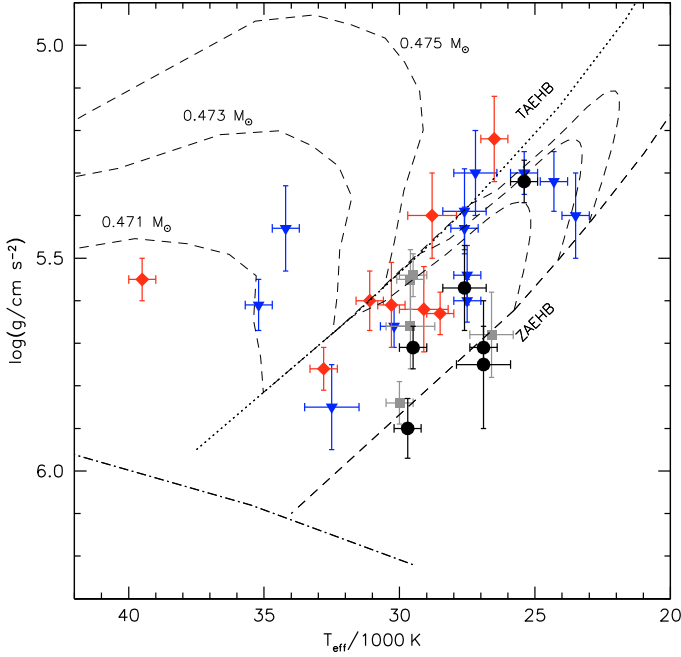
Fig. 11. Mass of the sdB primary HE 0532−4503 plotted against the mass of the unseen companion. The companion mass error is indicated by the dashed lines. The mass range of the CE ejection channel (Han et al. 2002) is marked with dotted vertical lines. The Chandrasekhar mass limit is plotted as solid horizontal line.

HE 0929−0424 and especially PG 1101+249 on the other hand would be near or below Hubble time and the total masses of the systems would most likely exceed the Chandrasekhar limit. If the companions should be massive white dwarfs of C/O composition, these binaries would be SN Ia progenitor candidates.

The companions of **PG 1432+159**, **HE 0532−4503** and **PG 1743+477** may be neutron stars as well as black holes as their masses exceed the Chandrasekhar limit even when errors are accounted for. Light curves have been obtained of both PG 1432+159 and PG 1743+477. The non-detection of reflection effects is perfectly consistent with compact companions (Maxted et al. 2004). In the case of PG 1743+477 only a lower limit for the companion mass could be derived. Due to their short orbital periods the companions in PG 1432+159 as well as in HE 0532−4503 will merge in a few billion years at most. Since the average lifetime on the EHB is only 100 Myr the sdBs will evolve to white dwarfs in the meantime. The outcome of a merger between a white dwarf and a neutron star or a black hole is unclear. Such systems may be progenitors for gamma-ray bursts or more exotic astrophysical transients (see discussion in Badenes et al. 2009).

In the case of **PG 1232−136** only a lower limit can be given for the companion mass (>6.0 $M_\odot$) which is higher than all theoretical NS masses. The companion of this sdBs may therefore be a BH.

7.4. Distribution in the T_{eff}-log g-plane

Figure 12 shows the distribution of the 31 solved binaries in the T_{eff}-log g-diagram. Within their error bars most of the sdB primaries are associated with the EHB as expected. Only three of them (BPS CS 22169−0001, KPD 1930+2752, KPD 1946+4340) have evolved beyond the TAEHB. No trends

Fig. 12. $T_{\mathrm{eff}} - \log g$-diagram; same as Fig. 2 but restricted to the sample which could be solved under the assumption of synchronisation. The helium main sequence and EHB band are superimposed with EHB evolutionary tracks from Dorman et al. (1993) labelled with their masses. Binaries with confirmed late main sequence or brown dwarf companions are plotted as filled diamonds, binaries with confirmed white dwarf companions with filled triangles. Hot subdwarfs where the companion could be a main sequence star or a white dwarf are marked with solid rectangles. The filled circles mark the sdBs with putative massive compact companions.

Fig. 13. $T_{\mathrm{eff}} - \log g$-diagram; same as Fig. 12 but restricted to the non-synchronised systems. The open squares mark binaries with orbital periods longer than 1.2 d. The filled one marks the system where synchronisation is not established despite its short orbital period.

with companion types can be seen. The location on the EHB is a function of the thickness of the stars' hydrogen layers. The thinner this layer is, the higher are T_{eff} and $\log g$ at the beginning of EHB-evolution and the more envelope mass has been lost during the CE-ejection. The efficiency of this process seems to be not much affected by the companion type. Companions of all types ranging from low mass M dwarfs or brown dwarfs to massive compact objects are scattered all over the EHB.

While the fraction of evolved sdBs is only 10% in the solved sample, two out of nine subdwarfs (22%) are found in binaries, which could not be solved under the assumption of synchronisation, are obviously not located on the EHB (see Fig. 13). A possible reason for this discrepancy is discussed in Sect. 11.1.

7.5. Distribution of companion masses

Figure 15 shows the low mass end of the companion mass distribution. Excluding the massive systems described in Sect. 7.3 the histogram mass distribution (Fig. 15) displays a peak at companion masses ranging from $0.2-0.4\,M_\odot$. Most of the low mass objects $<0.4\,M_\odot$ have been identified as M dwarfs. The bona fide white dwarf companions seem to peak at masses ranging from $0.4\,M_\odot$ to $0.8\,M_\odot$. Because close binary evolution is involved, there should be deviations from the normal mass distribution of single white dwarfs, which shows a characteristic peak at an average mass of $0.6\,M_\odot$. We therefore conclude that the mass distribution of the restricted sample looks reasonable and no obvious systematics can be seen. The high fraction of massive compact companions (up to 20% of our sample) on the other hand looks suspicious.
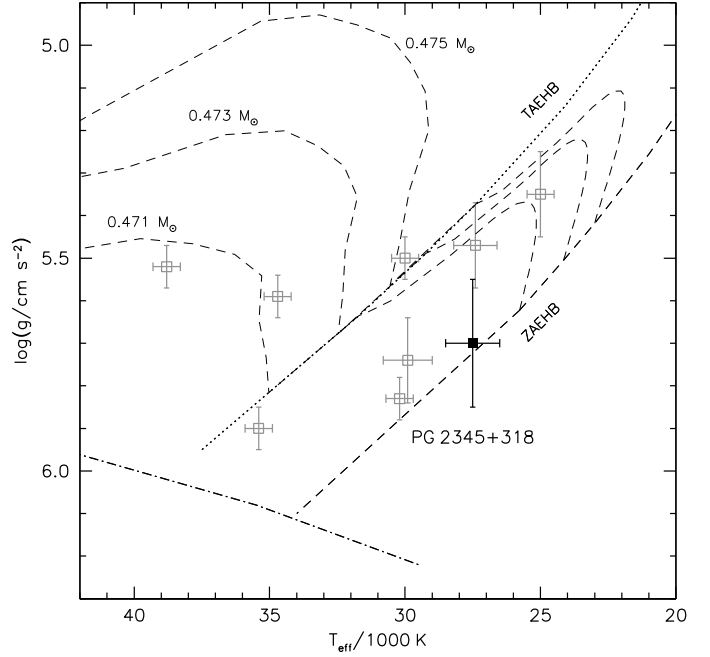
As the companion mass depends on the primary mass, the companion masses would be lower, if the primaries' masses were overestimated. We have adopted the masses of the sdB primaries to range from $0.43\,M_\odot$ to $0.47\,M_\odot$ as suggested by the models of Han et al. (2002, 2003) and backed-up by asteroseismology. However, the minimum mass of a core helium burning star can be as small as $0.3\,M_\odot$.

In Fig. 16 the companion mass distribution is plotted under the extreme assumption that all sdBs have this minimum mass for core helium burning (or the minimum mass allowed by other constraints). Looking at the low mass regime and comparing the distribution with Fig. 15 one immediately notices that this assumption leads to unphysical results. The distribution of low mass companions peaks at masses lower than $0.4\,M_\odot$, which is very unlikely especially for white dwarf companions.

Under this extreme assumption only the companion of PG 1232−136 remains more massive than the Chandrasekhar limit. Furthermore the companions of PG 1743+477 and HE 0532−4503 still are more massive than $1.0\,M_\odot$ in this case. With just slightly higher sdB masses the companion masses would exceed the Chandrasekhar limit.

7.6. The inclination problem

By plotting the companion masses versus inclination angles (Fig. 18) an anomaly becomes apparent. While the systems with low mass companions cover all inclination angles with a slight preference for high inclinations, the systems with massive compact companions are found at low inclinations between 15° and 30°.

Our sample has been drawn from the catalogue of Ritter & Kolb (2003), which is a compilation extracted from literature and not a systematic survey. Hence selection effects can not be quantified. Most of the low-mass, high-inclination systems have been discovered by photometry (eclipses and reflection effect),
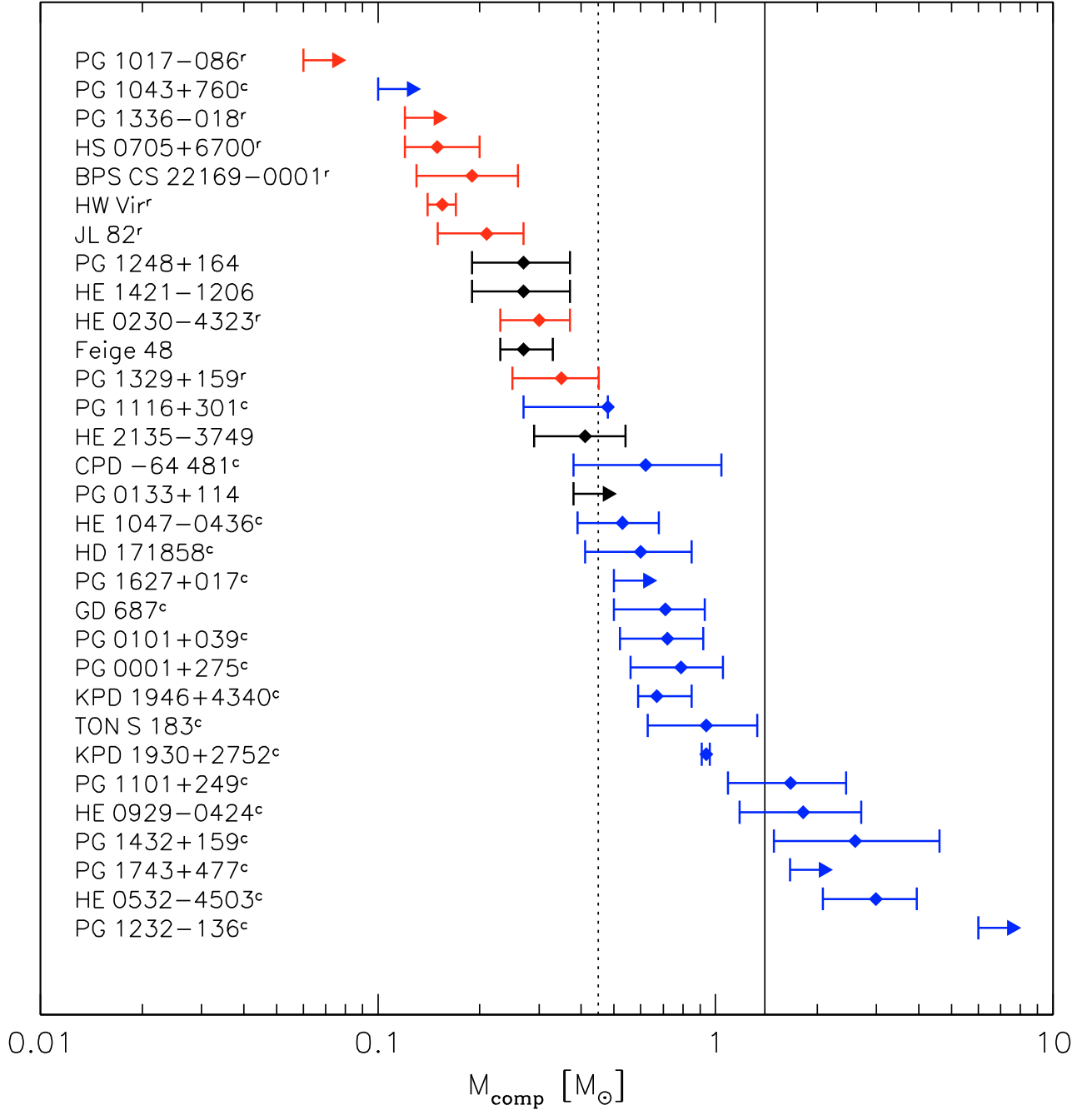
Fig. 14. Mass ranges for the unseen companions of 31 binaries under the assumption of synchronisation (see Table 4). The companion mass ranges are derived for the most likely sdB mass range of $0.43-0.47\ M_\odot$. The dashed vertical line marks the upper limit to the mass of main-sequence companions. Main-sequence stars with higher masses would be visible in the spectra and can be excluded, the solid vertical lines marks the Chandrasekhar mass limit. [r] Binaries with reflection effect detected in their light curves. The companions are either late M stars or brown dwarfs. [c] Binaries with compact companions like white dwarfs, neutron stars or black holes.

while all others stem from radial velocity surveys. The radial velocity technique is biased against low inclinations and low masses. Hence, massive systems at high inclinations should be found most easily. However, except for KPD 1930+2752, there is no high inclination object among the subsample of massive compact companions. One may speculate that such systems may have been overlooked, because their spectra may look peculiar due to orbital smearing and are therefore not classified as sdB stars.

We refrain from further speculations about selection effects and proceed to search for an evolutionary scenario that can

explain the formation of sdB binaries with neutron star or black hole companions.

8. The formation of sdB+NS/BH binaries

Neutron stars and stellar-mass black holes are the remnants of massive stars ending their lives in supernova explosions. Detecting these exotic objects is possible when they are in a close orbit with another star. If matter is transferred from the companion star to the compact object, X-rays are emitted. Not many neutron stars or stellar mass black holes could be found up
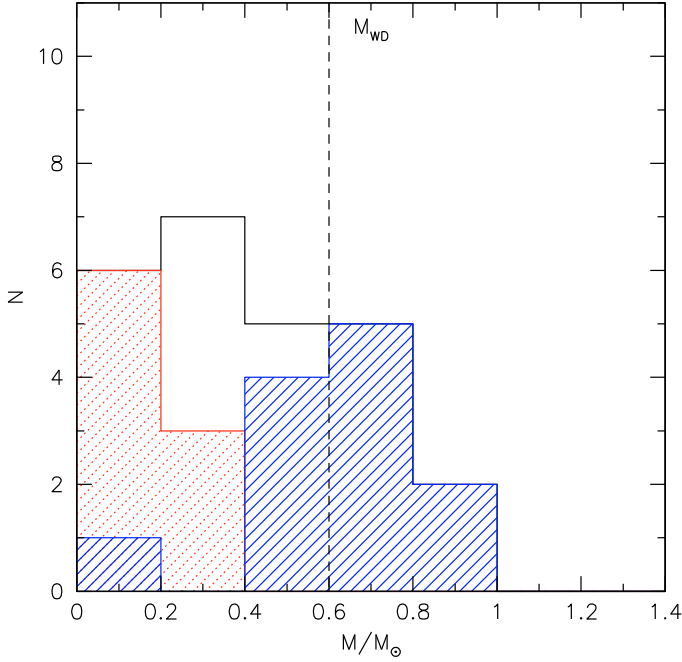
Fig. 15. Companion mass distribution of the binaries with low mass companions (Table 4, Fig. 14). The solid histogram shows the fraction of subdwarfs with confirmed white dwarf companions, the dashed histogram the detected M dwarf companions. The dashed vertical line marks the average white dwarf mass.
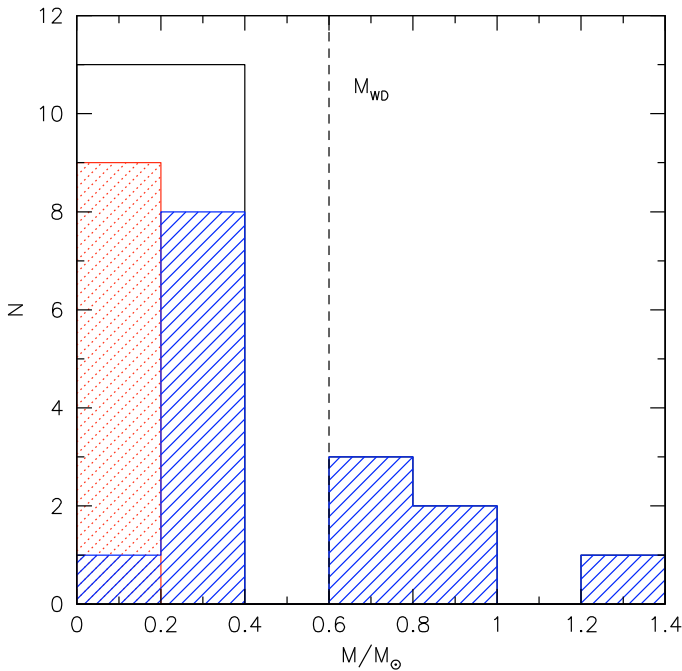

Fig. 16. Mass distribution of the unseen companion stars (see Fig. 15). The lowest possible companion mass is plotted against the total number of binaries under the assumption of the lowest possible sdB mass.

to now. On the other hand evolved, non-interacting binaries containing such objects should exist, since X-ray binaries only represent a relatively short phase of stellar evolution. Without ongoing mass transfer the companion remains invisible, but should be detectable indirectly from the reflex motion of the visible star. Badenes et al. (2009) discovered a massive compact companion to a white dwarf and concluded that this companion is likely to

be a neutron star. But Marsh et al. (2010) convincingly showed that the system is a double degenerate system consisting of a low mass and a very high mass WD. Kulkarni & van Kerkwijk (2010) performed an independent analysis with similar results. In this section the question whether sdB stars with hidden neutron star or black hole companions do exist is discussed in detail.

The existence of sdB+NS/BH systems requires an appropriate formation channel. The evolution that leads to such systems requires an initial binary, consisting of a primary star that is sufficiently massive to produce a neutron star or black hole, and a companion, the progenitor of the hot subdwarf, of typically several solar masses. The initial orbital period has to be quite large (a few to 20 years), so that mass transfer only starts late in the evolution of the star, and these systems generally experience two mass-transfer phases and one supernova explosion (see Fig. 17). The short orbital periods observed for our systems imply that the second mass-transfer phase from the red giant progenitor of the subdwarf to the compact companion had to be unstable, leading to a common-envelope and spiral-in phase of the compact object. The condition for unstable mass transfer constrains the mass of the progenitor to be larger than the mass of the compact object (otherwise, mass transfer would be stable and lead to a much wider system, Podsiadlowski et al. 2002). Figure 17 illustrates the evolution that leads to systems of this type for two typical examples. While this scenario can explain most of our systems with high-mass compact components, the inferred masses of the putative black hole in PG 1232−136 is larger than we would estimate ($\leq 3\,M_\odot$) for a $0.5\,M_\odot$ sdB star. This may suggest that this system has experienced another mass-transfer phase after the two common-envelope phases in which mass was transferred from the sdB star to the compact object. It should also be noted that, while we assume here that the mass of the subdwarf is $\sim 0.5\,M_\odot$, consistent with the properties of the observed systems, the sdB mass range allowed by this scenario is $0.3-1.1\,M_\odot$ for the neutron-star systems and $0.5-1.1\,M_\odot$ for the black-hole systems. Compared with the mass range of $0.3-0.7\,M_\odot$ for the standard evolutionary channel (Han et al. 2002, 2003), the subdwarf may therefore be more massive. An independent determination of the sdB mass (e.g. by obtaining parallaxes) could therefore help to verify this scenario.

At the beginning of the second mass-transfer phase, these systems are expected to pass through a short X-ray binary phase, lasting $\sim 10^5$ yr, in which a neutron star may accrete up to $\sim 10^{-3}\,M_\odot$ and become a moderately recycled millisecond pulsar (Podsiadlowski et al. 2002). This links these system to the X-ray binary population (in a sense, they are failed low-mass X-ray binaries). Population synthesis estimates (Pfahl et al. 2003) suggest that up to one in 10^4 stars in the Galaxy experience this evolution, implying that of order 1% of all hot subdwarfs should have neutron-star or black-hole companions. This means that tens of thousands of these systems could exist in the Galaxy compared to just about 300 known X-ray binaries. The binary PSR J1802−2124, which consists of a millisecond pulsar and a CO white dwarf in close orbit ($P = 0.7$ d, $M_{WD} = 0.78\,M_\odot$) may have evolved in a similar way (Ferdman et al. 2010).

Part II: Synchronisation – theory and empirical evidence

9. Orbital synchronisation of sdB binaries

The results presented above are based on the assumption of tidal synchronisation. Since especially the discovery of sdB+NS/BH systems challenges our understanding of stellar evolution, it is

Formation of subdwarfs with neutron stars
Initial binary: $M_1 = 15\,M_\odot$, $M_2 = 3\,M_\odot$, $P_{orb} \sim 4\,yr$.

Formation of subdwarfs with black holes
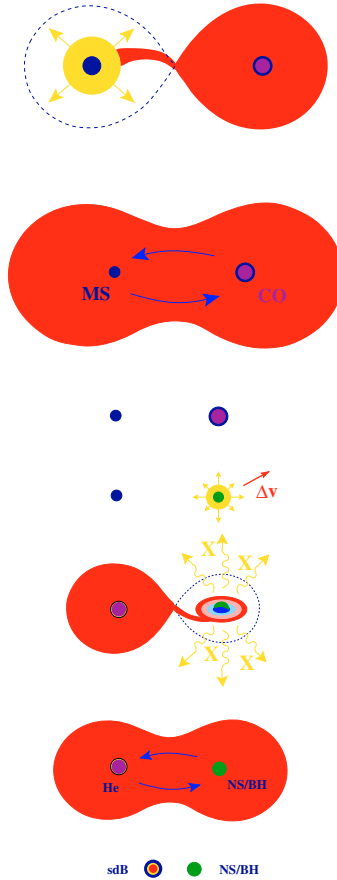*Initial binary: $M_1 = 30\,M_\odot$, $M_2 = 5\,M_\odot$, $P_{orb} \sim 10\,yr$.*

First unstable mass transfer (when the primary is a red supergiant; case C transfer) leading to a common-envelope and spiral-in phase.

First unstable mass transfer (when the primary is a red supergiant; case C transfer) leading to a common-envelope and spiral-in phase.

Helium-star binary with $M_{He} = 5\,M_\odot$ and $M_2 = 3\,M_\odot$, $P_{orb} = 10$ d.

Supernova (Type Ib/c) of the primary, producing a neutron star with $M_{NS} \simeq 1.4\,M_\odot$ and $M_2 = 3\,M_\odot$ in a highly eccentric orbit with $P_{orb} \sim 0.5\,yr$.

Helium-star binary with $M_{He} = 10\,M_\odot$ and $M_2 = 5\,M_\odot$, $P_{orb} = 20$ d.

Supernova (Type Ib/c) of the primary, producing a black hole with $M_{BH} \sim 4\,M_\odot$ and $M_2 = 5\,M_\odot$ in a highly eccentric orbit with $P_{orb} \sim 1\,yr$.

Second unstable mass transfer (when the secondary is a red giant; case B mass transfer) after a brief X-ray binary phase.

Second unstable mass transfer (when the secondary is a red giant; case B mass transfer) after a brief X-ray binary phase.

Helium-core burning hot subdwarf with $M_{sdb} \simeq 0.5\,M_\odot$ and a neutron star in an ultracompact orbit with $P_{orb} \simeq 10$ hr.

Helium-core burning hot subdwarf with $M_{sdb} \simeq 0.5 - 1\,M_\odot$ and a black hole in an ultracompact orbit with $P_{orb} \simeq 10$ hr.

Fig. 17. Schematic diagram of formation scenarios leading to hot subdwarf binaries with neutron-star (left hand panel) or black-hole (right hand panel) companions.

necessary to investigate whether this assumption holds in the case of sdBs. A thorough discussion of tidal synchronisation in sdB binaries both from the theoretical and the observational point of view is therefore given.

9.1. Theoretical timescales for synchronisation

Which mechanism is responsible for orbital synchronisation in binaries is still under debate. Theoretical timescales for synchronisation are given by Zahn (1977) and Tassoul & Tassoul (1992), but unfortunately they are not consistent for stars with radiative envelopes and convective cores like hot subdwarfs.

Zahn (1977) was the first to calculate synchronisation and circularisation timescales for main sequence stars in close binary systems. Observations of eclipsing binaries were in good agreement with his theoretical calculations for late type main-sequence stars with radiative cores and convective envelopes. Tidal friction caused by the equilibrium tide, which forms under the tidal influence of the close companion, is very efficient in this case because convection connects the inner regions of the stellar envelope with its surface. For radiative envelopes another mechanism is needed to explain the observed degree of synchronism in early type main-sequence binaries. Dynamical tides, which are excited at the boundary layer between the convective core and the radiative envelope are thought to be radiatively damped at the stellar surface and to transfer angular momentum outwards. This mechanism turns out to be much less efficient and the predicted synchronisation timescales are too long to explain the degree of synchronism in some early type main-sequence stars (e.g. Giuricin et al. 1984).

Tassoul & Tassoul (1992) introduced another, hydrodynamical braking mechanism. Tidally induced meridional currents in the non-synchronous binary components should lead to synchronisation and circularisation of the system. This mechanism is very efficient, but it was debated whether it is valid or not (Rieutord 1992; Tassoul & Tassoul 1997). Claret et al. (1995, 1997) studied both mechanisms and compared them to the available observations. Due to the necessary calibration of many uncertain parameters a definitive answer as to which mechanism is in better agreement with observation could not be given.

Applying the theory of tidal synchronisation to sdB binaries is not an easy task. One of the key results of both theories is that tidal circularisation of the orbit is achieved after the companions are synchronised. This means that once an orbital solution is found and the orbit turns out to be circular, both companions can be considered as synchronised without knowing their rotational properties. This simple law cannot be used in the case of sdBs. The reason is that close binary sdBs were formed via the CE ejection channel. The common envelope phase is very efficient in circularising the orbit and all known close binary sdBs have circular orbits or show only small eccentricities ($\epsilon \leq 0.06$; Edelmann et al. 2005; Müller et al. 2010; Napiwotzki et al., in prep.).
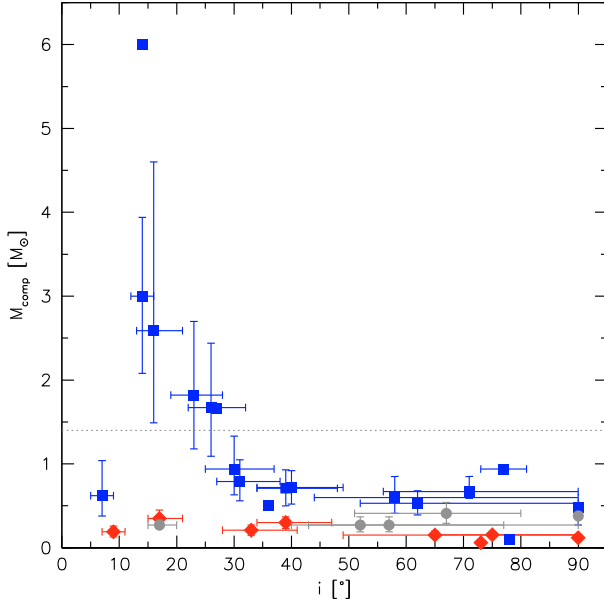
Fig. 18. Companion mass versus inclination. The solid squares mark compact companions (WD/NS/BH), the solid diamond MS or BD companions. The solid circles mark objects where both companion types are possible.

Stellar structure plays an important role. The synchronisation timescale of Zahn (1977) scales with $(R_C/R)^8$, where R_C is the radius of the convective core and R the stellar radius. The larger the convective core of a star, the shorter the time span until synchronisation is reached.

In order to estimate the synchronisation times of the analysed binaries we used the formulas of Zahn (1977) and Tassoul & Tassoul (1992).

$$t_{sync}(\text{Zahn}) = 52^{-5/3} \left(\frac{R^3}{GM} \right)^{1/2} \left(\frac{I}{MR^2} \right)$$
$$\times \frac{(1+q)^{5/6}}{q^2} E_2^{-1} \left(\frac{a}{R} \right)^{17/2}. \tag{5}$$

Here $M = M_{sdB}$, $R = R_{sdB}$, $q = M_{comp}/M_{sdB}$, a is the separation of the companions, which can be calculated from the measured orbital parameters using Kepler's third law, and I is the moment of inertia of the sdB star. We adopted the canonical sdB mass ($M_{sdB} = 0.47\,M_\odot$) for these calculations. E_2 is a tidal coefficient which is very sensitive to the structure of the star, especially the size of the convective core. Here we use the first approximation of Zahn (1977) $E_n = (R_C/R)^{2n+4}$ and adopt $R_C/R \simeq 0.15$ and $\frac{I}{MR^2} \simeq 0.04$ derived from sdB models calculated by Han (priv. comm.). For these models a hydrogen layer mass of $10^{-4}\,M_\odot$ was chosen consistent with result from asteroseismology (e.g. Charpinet et al. 2008).

$$t_{sync}(\text{Tassoul}) = 5.35 \times 10^{2+\gamma-N/4} \frac{1+q}{q} L^{-1/4}$$
$$\times M^{5/4} R^{-3} P^{11/4}. \tag{6}$$

In this equation M, R (solar units) and q are defined in the same way as above. P is the orbital period in days. The luminosity $L = 4\pi\sigma R^2 T_{eff}^4$ can be calculated using the T_{eff} measurements given in Table 1. The parameter N is connected with the different ways of energy transport within the outer layers of the stellar envelope. It is assumed to be zero in stars with radiative envelopes.

The parameter γ can be adjusted to account for large deviations from synchronism and contributions of both companions. Here the value $\gamma = 1.6$ used by Claret et al. (1995) was chosen. It has to be noted that this approach is only a crude approximation. As stated by Claret et al. (1997), the differential equations which govern the orbital parameters of a binary must be integrated. For this EHB evolution has to be taken into account. A detailed study of this problem is beyond the scope of this paper and we shall use Eqs. (5) and (6) to estimate the timescale of synchronisation.

It has to be pointed out that both theories predict the synchronisation timescale to increase strongly with increasing orbital period and to decrease with increasing sdB radius as $t_{sync} \sim P^\alpha$ and $t_{sync} \sim R^{-\beta}$. In the theory of Zahn (1977) the exponents are $\alpha = 17/3$ and $\beta = 9$, while the Tassoul & Tassoul formula gives $\alpha = 11/4$ and $\beta = 3$. In addition the synchronisation timescale decreases as the mass ratio increases. Hence it will take lower mass companions longer to synchronise the sdB star if the other parameters are constant.

9.2. Synchronisation of our sample

The synchronisation time scale depends strongly on orbital period and radius. Because the radii of the sdBs differ only little we display the results of our calculations as a function of orbital period in Fig. 19. The synchronisation timescales are given in units of the average EHB lifetime ($t_{EHB} \simeq 10^8$ yr; Dorman et al. 1993). A binary is thought to be synchronised, if the EHB lifetime is much longer than the synchronisation time. Due to the larger exponents α and β the slope of the relations is steeper and the scatter larger for the Zahn (1977) theory compared to the one proposed by Tassoul & Tassoul (1992). What can be seen immediately is that the timescales of Zahn (1977) and Tassoul & Tassoul (1992) differ by 2−8 orders of magnitude. Observational evidence is needed to constrain the timescales of tidal synchronisation in close binary sdBs.

For periods shorter than $\simeq 0.3$−0.4 d both theories predict synchronised rotation and are consistent with our observations. In the period range 0.4−1.2 d only the synchronisation times of Tassoul are consistent with observation, while the timescales of Zahn quickly exceed Hubble time. If the orbital periods exceed $\simeq 1.2$−1.6 d the assumption of synchronisation does not yield consistent results any more, although the timescales calculated with the prescription of Tassoul & Tassoul (1992) would still predict synchronised rotation.

According to our results, the period limit where synchronisation breaks down, lies near 1.2 d. The binaries HE 2150−0238 ($P = 1.32$ d) and PG 1512+244 ($P = 1.2$ d) cannot be solved consistently although their periods are only slightly longer than that of HE 1047−0436 (1.21 d) and PG 0133+114 (1.24 d), which can be solved.

Despite its long period, HD 171858 can be solved consistently, making it the longest period ($P = 1.6$ d) object in our sample that is synchronised. Why is this? Besides the orbital period the size of the star matters: The larger the star, the shorter the synchronisation time (see Eqs. (5) and (6)). The gravity of HD 171858 is lower than that of all other stars with periods ranging from 1.2 d to 1.6 d by a factor of 2 at least. Hence its radius is larger and synchronisation can be achieved more quickly than in the other stars of slightly shorter periods.

[CW 83] 1735+22 stands out among the longer-period binaries, because its projected rotational velocity (44 km s^{-1}) is unusually high. Because of its period ($P = 1.28$ d) it is not
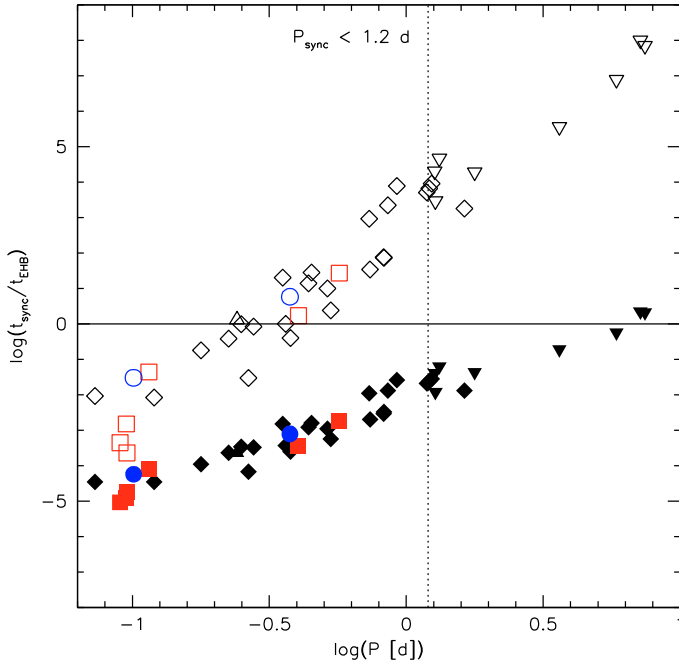
Fig. 19. Observed orbital period is plotted against the synchronisation times of Zahn (1977, open symbols) and Tassoul & Tassoul (1992, filled symbols) both in units of the average lifetime on the EHB (10⁸ yr, Dorman et al. 1993). The solid horizontal line marks the border between synchronisation within the EHB lifetime and synchronisation times longer than the EHB lifetime. The squares mark sdB binaries, where the primaries have been proven to be synchronised by light curve analysis of eclipsing or ellipsoidal variable systems. The circles mark binaries where synchronisation could be shown by asteroseismology. The systems marked with diamonds could be solved consistently under the assumption of synchronisation, while the systems marked with downward triangles rotate faster than synchronised. PG 2345+318 is the only sdB in our sample that rotates slower than synchronised. It is marked with an upward triangle.

necessarily expected to be synchronised. This system is discussed in detail in Sect. 11.1.

We also found that the short period binary PG 2345+318 ($P = 0.24$ d) rotates slower than synchronised. This peculiar system is discussed in detail in Sect. 11.2.

In general the synchronisation mechanism of Zahn (1977) is not efficient enough to explain the observed level of synchronisation, while the mechanism of Tassoul & Tassoul (1992) on the other hand appears to be much too efficient. Nevertheless, care has to be taken interpreting these results, because both theories give timescales for the synchronisation of entire stars from the core to the surface, while only the rotation at the surface can be measured from line broadening. Goldreich & Nicolson (1989) showed that in stars with radiative envelopes and Zahn's braking mechanism at work, the synchronous rotation proceeds from the surface towards the core of the star. This means that the outer layers are synchronised faster than the rest of the star. This effect would explain the discrepancy between Zahn's theory and our results at least to a certain extent. Unfortunately it was not possible to quantify this effect so far (see e.g. review by Zahn 2005).

Tidal synchronisation does not necessarily lead to an equality of orbital and rotational period. Higher spin resonances are possible and would change the derived parameters significantly (in case of the planet Mercury the ratio of orbital and rotational period is 3/2). To fall into a higher resonance, the binary

eccentricity has to be high at some point of its evolution. But close sdB binaries underwent at least one common envelope phase (maybe two in case of compact companions), which led to a circularisation of the orbit. The small eccentricities in some of our programme binaries reported by Edelmann et al. (2005) and Napiwotzki et al. (in prep.) are considered to be still consistent with this scenario. For these reasons, higher resonances are unlikely to occur in this evolutionary channel.

10. Empirical evidence for synchronisation

The timescale of the synchronisation process is highly dependent on the tidal force exerted by the companion. If the companion is very close and the orbital period therefore very short, synchronisation is established much faster than in binaries with longer orbital periods. If an sdB binary with given orbital period is proven to be synchronised, all other sdB binaries with shorter orbital periods should be synchronised as well. Although the timescales also scale with sdB radius and companion mass, the orbital period is the dominating factor because sdB radii differ only little and the dependence on companion mass is not so strong.

10.1. Eclipsing and ellipsoidal variable systems

Eclipsing sdB binaries are of utmost importance to test the synchronisation hypothesis because the inclinations can be derived directly from their light curves. It has been shown in Sect. 7.1 that the parameters of the eclipsing sdB+dM binaries PG 1336−018, HS 0705+6700 and HW Vir are consistent with synchronised orbits. This essentially means that the calculated $v_{rot} \sin i$ for synchronous rotation, which can be obtained as described in Sect. 4 given the orbital period, the radius of the sdB and the inclination angle are known, is consistent with the measured value. In eclipsing systems, all these parameters can be measured.

This provides clear empirical evidence that at least the upper layers of the stellar envelopes are synchronised to the orbital motion of the eclipsing sdB binaries in our sample. We therefore conclude that all sdBs in close binaries with orbital periods up to 0.12 d should be synchronised as well.

Two well studied sdBs clearly show ellipsoidal variations in their light curves with periods exactly half the orbital periods (KPD 1930+2752, Billères et al. 2000; Maxted et al. 2001; Geier et al. 2007, is further discussed in Sect. 7.2; KPD 0422+5421, Koen et al. 1998; Orosz & Wade 1999, is not part of our sample). This alone is only an indication for tidal synchronisation, because the light curve variations have to be present at the proper orbital phases as well. To really prove synchronisation it is necessary that the stellar parameters determined independently from the light curve analysis are consistent with a synchronised orbit. This is the case for KPD 0422+5421 as well as KPD 1930+2752. Both ellipsoidal variable systems have very short periods of $\simeq 0.1$ d and high inclination. Otherwise ellipsoidal variations are very hard to detect.

Most compelling evidence for synchronisation in a binary system with a period considerably longer than that of the above mentioned systems is provided in the case of the eclipsing sdB+WD binary KPD 1946+4340 ($P = 0.404$ d). Bloemen et al. (2010) derived most accurate binary parameters from a spectacular high-S/N light curve obtained by the Kepler mission. These results are fully consistent with the constraints we put on this system (see Sect. 7.2). We therefore conclude that sdB binaries with periods shorter than $P \simeq 0.4$ d should be synchronised.

Furthermore, the sdB+WD binary PG 0101+039 ($P = 0.567$ d) shows very weak luminosity variations at half the orbital period detected in a 16.9 day long, almost uninterrupted light curve obtained with the MOST satellite (Randall et al. 2005). Geier et al. (2008a) showed that the sdB in this binary is most likely synchronised. The empirical lower limit for tidal synchronisation in close sdB binaries is therefore raised to $P \simeq 0.6$ d.

10.2. Asteroseismology

An independent method to prove orbital synchronisation is provided by asteroseismology. Van Grootel et al. (2008) were able to reproduce the main pulsation modes of the short period pulsating sdB in the binary Feige 48 ($P \simeq 0.38$ d), derived the surface rotation from the splitting of the modes and concluded that the subdwarf rotates synchronously.

Charpinet et al. (2008) reach a similar conclusion for the short period eclipsing binary PG 1336−018 ($P \simeq 0.10$ d). Furthermore they probed the internal rotation of the star below the surface layers by applying a differential rotation law and showed that the sdB rotates as a rigid body at least down to $0.55\,R_{\rm sdB}$. The remarkable consistency of the binary parameters derived by asteroseismology (Charpinet et al. 2008), binary light curve synthesis (Vučković et al. 2007) and the analysis presented here has to be pointed out again (see Sect. 7.1). Asteroseismic analyses revealed that sdB binaries up to orbital periods of about 0.4 d are synchronised. We therefore conclude that all sdBs in close binaries with shorter periods should be synchronised as well.

11. Synchronisation challenged

In Sect. 9.2 we have shown that synchronisation in our sample has been established for binaries with periods below $\simeq 1.2$ d. This is corrobated by the theory of synchronisation although different version of the theory give vastly different results. Empirical evidence sets a limiting period of 0.6 d. About half of our sample has periods below that limit and should therefore be synchronised. These arguments are correct for the sample but may not hold for individual objects. We envisage two options: The subdwarf may not be core helium-burning (Sect. 11.1). Or an individual EHB star may be too young to have reached synchronisation (Sect. 11.2).

11.1. [CW 83] 1735+22 and post-RGB evolution

The only sdB star known not to burn helium in the core is the single-lined close binary HD 188112 (Heber et al. 2003). According to its atmospheric parameters it is situated well below the EHB (see Fig. 20). By interpolation of evolutionary tracks from Driebe et al. (1998) a mass of $0.23\,M_\odot$ was derived, which could be verified directly, because an accurate parallax of this object was obtained by the Hipparcos satellite.

The different evolution of so called post-RGB objects like HD 188112 compared to EHB stars should affect their rotational properties. Post-RGB stars constantly shrink during their evolution towards the WD cooling tracks. Since these stars are not expected to lose angular momentum during the contraction, they have to spin up. In contrast to this a core helium-burning sdB star expands by a factor of about two within $\simeq 100$ Myr and is expected to spin down. Besides HD 188112 some other objects are also considered to belong to this class (see Fig. 20).
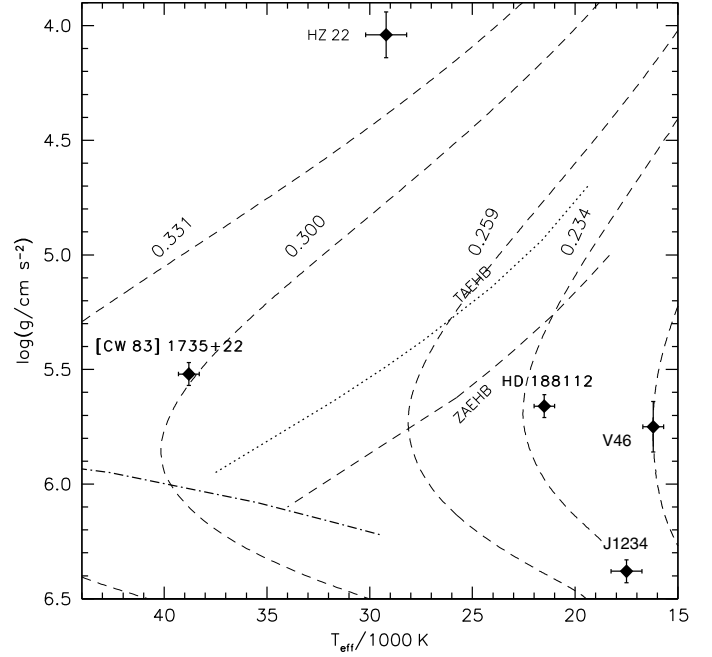

Fig. 20. $T_{\rm eff} - \log g$-diagram similar to Fig. 2. The black filled diamonds mark the known post-RGB binaries HD 188112 (Heber et al. 2003), NGC 6121−V46 (V46 for short, O'Toole et al. 2006), HZ 22 (Schönberner 1978; Saffer et al. 1997) and SDSS J123410.37−022802.9 (J1234 for short, Liebert et al. 2004). The candidate post-RGB system [CW83] 1735+22 is included as well. The helium main sequence and the EHB-band are superimposed with post-RGB evolutionary tracks from Driebe et al. (1998) labelled by their masses.

The post-RGB scenario may explain the unusual properties, especially the fast rotation, of the sdB binary **[CW 83] 1735+22** (see Sect. 9.2). The star is among the hottest in our sample and it lies far from the EHB band (see Fig. 20). According to the mass tracks of Driebe et al. (1998) [CW 83] 1735+22 would have a mass of about $0.3\,M_\odot$ (see Fig. 20). Such a star should shrink by a factor of 5.5 within 0.3 Myr (Driebe et al. 1998), which is much shorter than the synchronisation time. Hence we regard its high projected velocity as strong evidence that [CW 83] 1735+22 is a post-RGB star just like HD 188112. Since the lifetime of such an object is predicted to be only a few million years, such stars should be rare. The predicted low mass of [CW 83] 1735+22 can be verified in the way described in Heber et al. (2003) as soon as the GAIA mission will have measured an accurate trigonometric parallax of this star.

One may speculate that the different rotational properties of post-RGB stars may have an influence on the synchronisation process if they are in close binary systems. The spin-up caused by the shrinkage of the star may counteract the spin-down caused by the tidal influence of the companion. Should post-RGB stars have longer synchronisation timescales than EHB stars this may be invoked as a convenient explanation for the putative high fraction of sdB binaries with massive compact companions. If these binaries should have post-RGB primaries and should not be synchronised, the derived companion masses would be wrong.

This scenario is considered to be unlikely. First of all, we would expect post-RGB stars to rotate faster than synchronised. For the putative sdB+NS/BH systems low projected rotational velocities are measured. If the sdBs should rotate even faster than synchronised, the inclination angle would be even lower and the derived companion masses would go up.
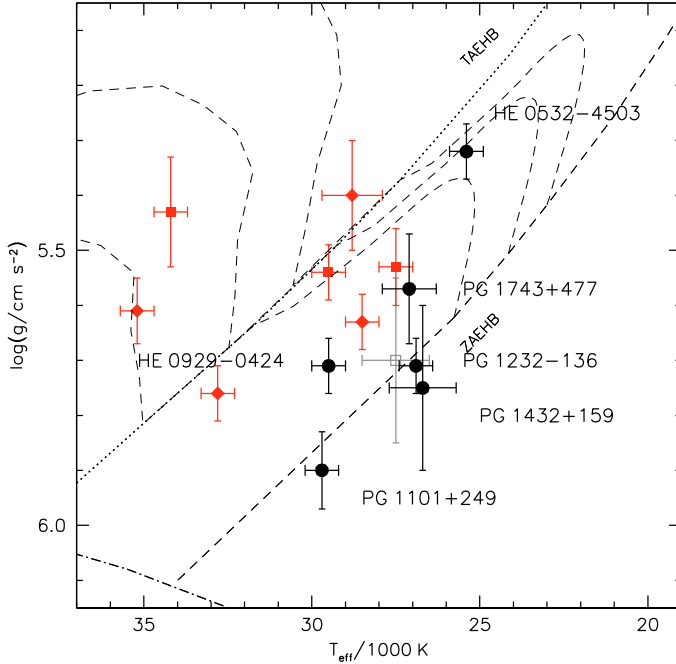
Fig. 21. $T_{\mathrm{eff}} - \log g$-diagram, same as Fig. 2 but restricted to the massive systems (black filled circles) described in Sect. 7.3 and supplemented by short-period systems ($\simeq 0.1$ d, filled diamonds) where synchronisation has been proven empirically. The two filled squares mark the longer period binaries Feige 48 ($\simeq 0.38$ d), KPD 1946+4340 ($\simeq 0.40$ d) and PG 0101+039 ($\simeq 0.57$ d), which are known to be synchronised. The open square marks the non-synchronised binary PG 2345+318. The helium main sequence and the EHB band are superimposed with EHB evolutionary tracks from Dorman et al. (1993) labelled by their masses.

Another strong argument against a post-RGB nature of the sdBs in the candidate systems with massive compact companions is their location in the $T_{\mathrm{eff}} - \log g$ diagram (see Fig. 21). All these binaries are found on or near the EHB, while the known post-RGB stars are obviously not concentrated near the EHB (see Fig. 20). We therefore conclude that the sdBs with putative massive compact companions are post-EHB rather than post-RGB stars.

11.2. The role of the stellar age

Up to now we have assumed that the sdB stars already have spent a significant part of their total life time on the EHB. In the canonical picture it might be possible to estimate the age of an individual star by comparing its position in the (T_{eff}, $\log g$)-diagram to EHB evolutionary tracks (e.g. Dorman et al. 1993), as the core mass is fixed at the core helium flash. In binary population models, however, a degeneracy between mass and age arises as there is a spread of sdB masses (see Zhang et al. 2009).

Because our sample stars nicely populate the canonical EHB band (see Figs. 2, 12, 13), we shall assume that a star is young if it is on or close to the zero-age extreme horizontal branch (ZAEHB) and old if not. Note that the speed of evolution along the EHB tracks is nearly constant.

We shall now explore whether some of our targets might possibly be too young to be synchronised. We shall start with PG 2345+318 and inspect the sample in the light of the lesson to be learnt.

11.3. PG 2345+318

PG 2345+318 is a short period (0.24 d) sdB binary. We derive a high companion mass of $1.9 \pm 0.7 \, M_\odot$ at an inclination angle of about $22°$ indicating that the companion is another massive compact object, i.e. a neutron star or a massive white dwarf. At such a low inclination eclipses are not expected to occur.

However, Green et al. (2004) presented a preliminary light curve of this star, and detected a shallow eclipse probably by a white dwarf[7]. Without the additional information from the light curve this object would therefore be identified as another candidate sdB binary with massive compact companion. The detection of eclipses immediately rules out this scenario. The inclination angle has to be near $90°$ and the companion a white dwarf with a mass of $0.38 \, M_\odot$ according to the constraint set by the binary mass function. This means that the sdB star in this binary rotates more slowly than synchronised and proves that such objects exist among binaries with short orbital periods. The most reasonable explanation for this may be that the system is very young and the synchronisation process not finished yet.

The atmospheric parameters of this star (see Table 1) place it indeed near the zero-age EHB (Fig. 21), although they have somewhat larger errors than most other stars due to the lack of high quality low resolution spectra (Saffer et al. 1994). But the light curve presented by Green et al. (2004) reveals more information, which corroborate this scenario. An interesting feature is the presence of a shallow reflection effect and a weak secondary minimum, which provides evidence that the white dwarf contributes significantly to the optical flux. This in turn means that the white dwarf must be young (assuming a luminosity of $0.5 \, L_\odot$ evolutionary tracks imply an age of the order of 10^6 yr) and is another piece of evidence that the system is too young to be synchronised. Since no light curve solution for PG 2345+318 is published yet, the discussion of this object must remain preliminary.

11.4. Are the systems with massive compact companions too young to be synchronised?

What are the implications for our candidate sample of sdB binaries with massive compact companions? The orbital periods of these binaries range from 0.26 d to 0.52 d where synchronisation should be established according to the results presented in Sects. 9.2 and 10. Given these short orbital periods, the binaries in question should be synchronised.

Even if the candidate systems were bona-fide EHB stars, they may just be too young to be synchronised. In Fig. 21 we plot the positions of the candidate systems with compact companions and compare them to the calibrators Feige 48, PG 0101+039 and KPD 1946+4340. It is obvious that the first two of these synchronised sdBs lie closer to the terminal age EHB than to the zero age EHB. KPD 1946+4340 is already evolved from the EHB and most likely burning helium in a shell. These are indications that these binaries are relatively old. We also note that the position of PG 1743+477 nearly coincides with that of PG 0101+039. From this coincidence we would expect it to be synchronised and, hence, the constraint on the companion mass to be reliable.

We also plot the position of the non-synchronised system PG 2345+318 in Fig. 21 which lies near the zero-age EHB. PG 1232−136 and PG 1432+159 are found close to

---

[7] Besides KPD 0422+5421 (Orosz & Wade 1999), PG 0941+280 (Green et al. 2004) and KPD 1946+4340 (Bloemen et al. 2010) this is just the fourth such system known.

PG 2345+318 and near the zero-age EHB and thus may be rather young as well. The same holds for PG 1101+249 which is considerably hotter but also situated very near the zero-age EHB (ZAEHB).

The remaining candidate sdB binaries with putative massive compact companions are in a similar evolutionary stage as the synchronised systems in the middle of the EHB band. We conclude that some but not all sdBs in the candidate systems could be too young to have reached synchronisation.

12. Summary and outlook

We have analysed a sample of 51 sdB stars in close single-lined binary systems. This included 40 systems for which the orbital parameters have been determined previously. The sub-sample comprises half of all systems known so far. From high resolution spectra taken with different instruments the projected rotational velocities of these stars have been derived to an unprecedented precision. Accurate measurements of the surface gravities have mostly been taken from literature. Assuming orbital synchronisation and an sdB mass distribution as suggested by binary population synthesis models as well as by asteroseismology, the masses and the nature of the unseen companions could be constrained in 31 cases. Only in five cases we were unable to classify unambiguously. These companions may either be low mass main-sequence stars or white dwarfs. The companions to seven sdBs could be clearly identified as late M stars. One binary may have a brown dwarf companion. The unseen companions of nine sdBs are white dwarfs with typical masses, one WD companion has a very low mass.

In eight cases (including the well known system KPD1930+2752) the companion mass exceeds 0.9 $M_\odot$. Four of the companions even exceed the Chandrasekhar limit indicating that they may be neutron stars; even a stellar mass black hole is possible for the most massive companions.

The basic assumption of orbital synchronisation in close sdB binaries has been discussed in detail. Our analysis method yielded consistent results for binaries up to an orbital period of $\simeq$1.2 d. Theoretical timescales for synchronisation were calculated using two different approaches. The theory of Zahn (1977) was found to be too inefficient while that of Tassoul & Tassoul (1992) predicts too short timescales. The predictions from both theories are strongly discrepant, calling for empirical constraints.

Independent observational evidence for synchronisation in sdB binaries comes from light curve analyses of eclipsing, ellipsoidal deformed, and pulsating sdBs. Due to this evidence sdB binaries with periods shorter than $\simeq$0.6 d should be synchronised. This includes all of the putative massive systems.

Hence, an evolutionary model for the origin of sdB stars with neutron star or black hole companions was devised indicating that common envelope evolution is indeed capable of producing such systems, though at a lower rate than observed. An appropriate formation channel includes two phases of unstable mass transfer and one supernova explosion.

The distribution of the inclinations of the systems of normal mass appears to be consistent with expectations, whereas a lack of high inclinations became obvious for the massive systems.

There is one star in the sample which rotates fast despite its rather long orbital period. This as well as its position far from the EHB band hints at a post-RGB nature. The post-RGB stars are expected to be spun-up due to their ongoing contraction.

The larger number of putative massive companions in low inclination systems is puzzling. Therefore, we investigated alternative interpretations. The fraction of massive unseen companions can only be lowered, if the sdBs themselves have masses much lower than the anticipated range of 0.43−0.47 $M_\odot$ for EHB stars. Evolutionary calculations showed that EHB stars with masses as low as 0.30 $M_\odot$ can be formed if helium ignites under non-degenerate conditions but should be very rare. Assuming such low sdB masses, only one unseen companion remains more massive than the Chandrasekhar limit. This fraction of 3% is roughly consistent with theoretical predictions. Whether the sdB mass is small or not can be checked directly as soon as accurate parallaxes of these relatively bright stars will become available through the GAIA mission.

The putative massive sdB systems might not be synchronised if their age is much less than anticipated. That this can happen is witnessed by PG 2345+318, a short-period sdB binary in our sample, that we would have classified as a low-inclination massive system as well, if it were not proven by eclipses to be highly inclined. Hence the system is not synchronised despite of its short period (0.24 d). Due to a degeneracy between mass and age, it is difficult to estimate the sdB's age without knowing its mass. Adopting the canonical mass, we nevertheless estimated the stars' ages from their position in the EHB band. Indeed, PG 2345+318, is located right on the zero-age EHB as are the massive candidates PG 1232−136, PG 1432+159 and PG 1101+249. These stars may possibly be too young to have reached synchronisation. Hence the companion masses we derived would be spurious. However, there is no indication that the other massive systems could be young.

Even if we dismiss three candidates because they may be too young and assume that the others are of low mass, PG 1743+477 and, in particular, HE 0532−4503 remain as massive candidates whose companions have masses close to or above the Chandrasekhar mass.

Different approaches may be chosen to directly verify the presence of neutron star or black hole companions in our candidate systems. None of the sdBs in our target systems fills its Roche lobe. No mass transfer by Roche lobe overflow to the unseen companion can occur and therefore no X-ray emission is expected. The ROSAT all-sky survey catalogue (RASS, Voges et al. 1999) has been checked and, indeed, no sources have been detected at the positions of any candidate sdB+NS/BH systems. The detection limit of this survey reaches down to about 10^{-13} erg cm^{-2} s^{-1}. However, sdB stars are expected to have weak winds. Hence accretion from the sdB wind might result in faint X-ray emission. This occurs in the bright sdO+WD system HD 49798 (Mereghetti et al. 2009). Although stellar wind mass loss rates in sdBs are predicted to be small ($<10^{-12}$ $M_\odot$ yr^{-1}, e.g. Vink & Cassisi 2002; Unglaub 2008), they may be sufficient to cause detectable X-ray flux powered by wind accretion. X-ray telescopes like Chandra or XMM-Newton may be sensitive enough to detect such weak sources. Pulsar signatures of rapidly spinning neutron star companions may be detectable with radio telescopes.

Tidal forces by the companion cause an ellipsoidal deformation of the primary in close binary systems. This deformation appears as a variation of light at half the orbital period. Two very close subdwarf binaries with orbital periods of $\simeq$2 h and high orbital inclination show light variations of about 1%, which can be detected from the ground. Performing binary light curve synthesis it was possible to derive the masses of the binary components (Orosz & Wade 1999; Geier et al. 2007). Signatures of ellipsoidal deformation in the light curves of binaries with longer orbital periods and lower inclination are much weaker ($\simeq$0.01%, Drechsel, priv. comm.; Napiwotzki et al., in prep.) and

therefore not detectable from the ground. The existence of such very shallow variations has been proven for the subdwarf binary PG 0101+039 with an orbital period of 13.7 h using a light curve of almost 17 d days duration taken with the MOST satellite. The ellipsoidal variation was found to be 0.025% (Geier et al. 2008a). The full potential of high precision photometry for the analysis of sdB binaries has most recently been demonstrated by Bloemen et al. (2010), who analysed a Kepler light curve of the eclipsing sdB+WD binary KPD 1946+4340. High precision light curves of the best candidates in our sample should be measured with HST. The nature of their unseen companion could then be clarified.

Most of the candidate massive systems have low orbital inclination. High inclination systems must exist as well. In this case a determination of the orbital parameters is sufficient to put a lower limit to the companion mass by calculating the binary mass function. If this lower limit exceeds the Chandrasekhar mass and no sign of a companion is visible in the spectra, the existence of a massive compact companion is proven without making any additional assumptions. The MUCHFUSS project (Massive Unseen Companions to Hot Faint Underluminous Stars from SDSS, Geier et al. 2010b) was launched in 2007. The aim of this project is to search for sdB binaries with massive compact companions at high inclinations in a sample of stars selected from the SDSS data base.

References

Ahmad, A., Jeffery, C. S., & Fullerton, A. W. 2004, A&A, 418, 275
Badenes, C., Mullally, F., Thompson, S. E., & Lupton, R. H. 2009, ApJ, 707, 971
Behr, B. 2003, ApJS, 149, 101
Berger, L., Koester, D., Napiwotzki, R., Reid, I. N., & Zuckerman, B. 2005, 444, 565
Billères, M., Fontaine, G., Brassard, P., et al. 2000, ApJ, 530, 441
Bloemen, S., Marsh, T. R., Østensen, R. H., et al. 2010, MNRAS, submitted
Charpinet S., Fontaine G., Brassard P., & Dorman B. 1996. ApJ, 471, L103
Charpinet, S., Fontaine, G., Brassard, P., et al. 2005, A&A, 443, 251
Charpinet, S., van Grootel, V., Reese, D., et al. 2008, A&A, 489, 377
Claret, A., & Cunha, N. C. S. 1997, A&A, 318, 187
Claret, A., Giménez, & Cunha, N. C. S. 1995, A&A, 299, 724
Dorman, B., Rood, R. T., & O'Connell, R. W. 1993, ApJ, 419, 596
Drechsel, H., Heber, U., Napiwotzki, R., et al. 2001, A&A, 379, 893
Driebe, T., Schönberner, D., Böcker, T., & Herwig, F. 1998, A&A, 339, 123
Edelmann, H. 2008, ASP Conf. Ser., 392, 187
Edelmann, H., Heber, U., & Napiwotzki, R. 1999, ASP Conf. Ser., 169, 546
Edelmann, H., Heber, U., & Napiwotzki, R. 2001, AN, 322, 401
Edelmann, H., Heber, U., Altmann, M., Karl, C., & Lisker, T. 2005, A&A 442, 1023
Ergma, E., Fedorova, A. V., & Yungelson, L. R. 2001, A&A, 376, L9
Farihi, J., Becklin, E. E., & Zuckerman, B. 2005, ApJS, 161, 394
Ferdman, R. D., Stairs, I. H., Kramer, et al. 2010, ApJ, 711, 764
Fleig, J., Rauch, T., Werner, K., & Kruk, J. W. 2008, A&A, 492, 565
Fontaine, G., Brassard, P., Charpinet, S., et al. 2008, ASP Conf. Ser., 392, 231
For., B.-Q., Green, E. M., O'Donoghue, D., et al. 2006, ApJ, 642, 1117
For, B.-Q., Green, E. M., Fontaine, G., et al. 2010, ApJ, 708, 253
Geier, S., Nesslinger, S., Heber, U., et al. 2007, A&A, 464, 299
Geier, S., Nesslinger, S., Heber, U., et al. 2008a, A&A, 477, L13
Geier, S., Heber, U., & Napiwotzki, R. 2008b, ASP Conf. Ser., 392, 159
Geier, S., Heber, U., Edelmann, H., Kupfer, T., Napiwotzki, R., et al. 2009a, JPhCS, 172, 012008
Geier, S., Edelmann, H., Heber, U., & Morales-Rueda, L. 2009b, ApJ, 702, L96
Geier, S., Heber, U., Kupfer, T., & Napiwotzki, R. 2010a, A&A, 515, 37
Geier, S., Hirsch, H., Tillich, A., et al. 2010b, A&A, submitted
Giuricin, G., Mardirossian, F., & Mezzetti, M. 1984, A&A, 135, 393
Green, E. M., Liebert, J. W., & Saffer, R. A. 1997, in Third Conference on Faint Blue Stars, ed. A. G. D. Philip, J. Liebert, R. Saffer, & D. S. Hayes, (Schenectady: L. Davis Press), 417
Green, E. M., Fontaine, G., Reed, M. D., et al. 2003, ApJ, 583, L31
Green, E. M., For, B., Hyde, E. A., et al. 2004, ApSS, 291, 267
Green, E. M., Fontaine, G., Hyde, E. A., For, B.-Q., & Chayer, P. 2008, ASP Conf. Ser., 392, 75
Goldreich, P., & Nicolson, P. D. 1989, ApJ, 342, 1079
Hamada, T., & Salpeter, E. E., 1961, ApJ, 134, 638
Han, Z., Podsiadlowski, P., Maxted, P. F. L., Marsh, T. R., & Ivanova, N. 2002, MNRAS, 336, 449
Han, Z., Podsiadlowski, P., Maxted, P. F. L., & Marsh, T. R. 2003, MNRAS, 341, 669
Heber, U. 1986, A&A, 155, 33
Heber, U. 2009, ARA&A, 47, 211
Heber, U., & Edelmann, H. 2004, Ap&SS, 291, 341
Heber, U., Reid, I. N., & Werner, K. 2000, A&A, 363, 198
Heber, U., Edelmann, H., Lisker, T., & Napiwotzki, R. 2003, A&A, 411, 477
Iben, I., & Tutukov, A. V. 1984, ApJ, 284, 719
Iben, I., & Tutukov, A. V. 1994, ApJ, 431, 264
Karl, C., Heber, U., Napiwotzki, R., & Geier, S. 2006, Balt. Astron., 15, 151
Kilkenny, D., Koen, C., O'Donoghue, D., & Stobie, R. S. 1997, MNRAS, 285, 640
Kilkenny, D., Koen, C., & Worters, H. 2010, MNRAS, 404, 376
Koen, C. 2007, MNRAS, 377, 1275
Koen, C. 2009, MNRAS, 395, 979
Koen, C., Orosz, J. A., & Wade, R. A. 1998, MNRAS, 300, 695
Koen, C., Kilkenny, D., Pretorius, M. L., & Frew, D. J. 2010, MNRAS, 401, 1850
Kudritzki, R.P., & Simon, K.P. 1978, A&A, 70, 653
Kulkarni, S. R., & van Kerkwijk, M. H. 2010, ApJ, 719, 1123
Lee, J. W., Kim, S.-L., Kim, C.-H., et al. 2009, ApJ, 137, 3181
Leibundgut, B. 2001, ARA&A, 39, 67
Lemke, M. 1997, A&AS, 122, 285
Liebert, J., Bergeron, P., Eisenstein, D., et al. 2004, ApJ, 606, L147
Lisker, T., Heber, U., Napiwotzki, R., Christlieb, N., Han, Z., et al. 2005, A&A, 430, 223
Livio, M. 2000, in Type Ia Supernovae: Theory and Cosmology, ed. J. C. Niemeyer, J. C., & J. W. Truran (Cambridge: University Press), 33
Marsh, T. R., Gaensicke, B. T., Steeghs, D., et al. 2010, ApJL, submitted [arXiv:1002.4677]
Maxted, P. F. L., Marsh, T. R., & North, R. C. 2000a, MNRAS, 317, L41
Maxted, P. F. L., Moran, C. K. J., Marsh, T. R., & Gatti, A. A. 2000b, MNRAS, 311, 877
Maxted, P. F. L., Heber, U., Marsh, T. R., & North, R. C. 2001, MNRAS, 326, 139
Maxted, P. F. L., Marsh, T. R., Heber, U., et al. 2002, MNRAS, 333, 231
Maxted, P. F. L., Morales-Rueda, L., & Marsh, T. 2004, Ap&SS, 291, 307
Mengel J.G., Norris J., & Gross P.G. 1976, ApJ, 204, 488
Mereghetti, S., Tiengo, A., Esposito, P., La Palombara, N., Israel, G. L., et al. 2009, Science, 325, 1222
Morales-Rueda, L., Maxted, P. F. L., Marsh, T. R., North, R. C., & Heber, U. 2003, MNRAS, 338, 752
Morales-Rueda, L., Maxted, P. F. L., Marsh, T. R., Kilkenny, D., & O'Donoghue, D. 2004, ASP Conf. Ser., 334, 333
Moran, C., Maxted, P. F. L., Marsh, T. R., Saffer, R. A., & Livio, M. 1999, MNRAS, 304, 535
Müller, S., Geier, S., & Heber, U. 2010, in Proc. Fourth Meeting on Hot Subdwarf Stars and Related Object, Shanghai, July 2009, Ap&SS, in press
Napiwotzki, R., Edelmann H., Heber U., Karl, C., Drechsel H., et al. 2001a, A&A 378, L17
Napiwotzki, R., Christlieb, N., Drechsel, H., et al. 2001b, AN, 322, 411
Napiwotzki, R., Christlieb, N., Drechsel, H., et al. 2003, ESO Msngr, 112, 25
Napiwotzki, R., Karl, C. A., Lisker, T., et al. 2004a, Ap&SS, 291, 321
Napiwotzki, R., Yungelson, L., Nelemans, G., et al. 2004b, ASP Conf. Ser., 318, 402
Orosz, J. A., & Wade, R. A. 1999, MNRAS, 310, 773
O'Toole, S. J., & Heber, U. 2006, A&A, 452, 579
O'Toole, S. J., Heber, U., & Benjamin, R. A. 2004, A&A, 422, 1053
O'Toole, S. J., Napiwotzki, R., Heber, U., et al. 2006, Balt. Astron., 15, 61
Perlmutter, S., Aldering, G., Goldhaber, G., et al. 1999, ApJ, 517, 565
Pfahl, E., Rappaport, S., & Podsiadlowski, Ph. 2003, ApJ, 597, 1036
Podsiadlowski, Ph., Rappaport, S., & Pfahl, E. D. 2002, ApJ, 565, 1107
Politano, M., Taam, R. E., van der Sluys, M., & Willems, B. 2008, ApJ, 687, L99
Randall, S. K., Matthews, J. M., Fontaine, G., et al. 2005, ApJ, 633, 460
Rauch, T., & Werner, K. 2003, A&A, 400, 271

Reed, M. D., & Stiening, R. 2004, PASP, 116, 506
Reed, M. D., Kawaler, S. D., Zola, S., et al. 2004, MNRAS, 348, 1164
Riess, A. G., Fillipenko, A. V., Challis, P., et al. 1998, AJ, 116, 1009
Rieutord, M. 1992, A&A, 259, 581
Ritter, H., & Kolb, U. 2003, A&A, 404, 301 (update RKcat7.12, 2009)
Rucinski, S. M. 2009, MNRAS, 395, 2299
Saffer, R. A., Bergeron, P., Koester, D., Liebert, J. 1994, ApJ, 432, 351
Saffer, R. A., Keenan, F. P., Hambly, N. C., Dufton, P. L., & Liebert, J. 1997, ApJ, 491, 172
Saffer, R. A., Livio, M., & Yungelson, L. R. 1998, ApJ, 502, 394
Sarazin, M., & Roddier, F. 1990, A&A, 227, 294
Schönberner, D. 1978, A&A, 70, 451
Shimanskii, V. V., Bikmaev, I. F., Borisov, N. V., et al. 2008, ARep, 52, 729
Soker, N. 1998, AJ, 116, 1308
Stark, M. A., & Wade, R. A. 2003, AJ, 126, 1455
Sweigart, A. V. 1997, in Proc. Third Conference on Faint Blue Stars, ed. A. G. D. Philip, J. Liebert, R. Saffer, & D. S. Hayes, 3

Tassoul, J.-L., & Tassoul, M. 1992, ApJ, 395, 259
Tassoul, M., & Tassoul, J.-L. 1997, ApJ, 481, 363
Telting, J. H., Geier, S., Østensen, R . H., et al. 2008, A&A, 492, 815
Unglaub, K. 2008, A&A, 486, 923
van Grootel, V., Charpinet, S., Fontaine, G., & Brassard, P. 2008, A&A, 483, 875
Vink, J. S., & Cassisi, S. 2002, A&A, 392, 553
Voges, W., Aschenbach, B., Boller, T., et al. 1999, A&A, 349, 389
Vučković, M., Aerts, C., Østensen, R., et al. 2007, A&A, 471, 605
Vučković, M., Østensen, R., Bloemen, S., Decoster, I., & Aerts, C. 2008, ASP Conf. Ser., 392, 199
Webbink, R. F. 1984, ApJ, 277, 355
Wood, J. H., & Saffer, R. A. 1999, MNRAS, 305, 820
Wood, J. H., Zhang, E.-H.& Robinson, E. L. 1993, MNRAS, 261, 103
Zahn, J.-P. 1977, A&A, 57, 383
Zahn, J.-P. 2005, ASP Conf. Ser., 333, 4
Zhang, X., Chen, X., & Han, Z. 2009, A&A, 504, L13